3566 J. Med. Chem. 2010, 53, 3566–3584
DOI: 10.1021/jm901846t

Journal of Medicinal Chemistry Article

How Well Can the Caco-2/Madin−Darby Canine Kidney Models Predict Effective Human Jejunal Permeability?†

Alex Avdeef*,‡ and Kin Y. Tam*,§

‡pION Inc., 5 Constitution Way, Woburn, Massachusetts 01801, and §AstraZeneca, Mereside, Alderley Park, Macclesfield, Cheshire SK10 4TG, U.K.

Received December 14, 2009

The study aimed to predict effective human jejunal permeability (P_{eff}) using a biophysical model based on parametrized paracellular, aqueous boundary layer, and transcellular permeabilities, and the villus-fold surface area expansion factor (k_{VF}). Published human jejunal data (119 P_{eff}, 53 compounds) were analyzed by a regression procedure incorporating a dual-pore size paracellular model. Transcellular permeability, scaled by k_{VF}, was equated to that of Caco-2 at pH 6.5. The biophysical model predicted human jejunal permeability data within the experimental uncertainty. This investigation revealed several surprising predictions: (i) many molecules permeate predominantly (but not exclusively) by the paracellular route, (ii) the aqueous boundary layer thickness in the intestinal perfusion *experiments* is larger than expected, (iii) the mucosal surface area in awake humans is apparently nearly entirely accessible to drug absorption, and (iv) the relative "leakiness" of the human jejunum is not so different from that observed in a number of published Caco-2 studies.

Introduction

Drug absorption from the gastrointestinal tract (GIT) includes the permeation of the dissolved therapeutic molecule across the intestinal barrier from the luminal fluid into the blood by the transcellular and/or paracellular route.[1−3] Over the past 20 years, measurements of the effective permeability, P_{eff},[a] of the human intestinal barrier have been published for 53 compounds (mostly drugs), using a single-pass perfusion of the proximal jejunum in awake subjects (mostly by the "gold standard" Loc-I-Gut technique); about 119 P_{eff} values have been published.[3−31] Because of the complexity and high cost of such in situ experiments, there is an ongoing effort to model the in vivo system by in vitro apparent permeability, P_{app}, measurements, e.g., using Caco-2 or Madin−Darby canine kidney (MDCK) cultured cell lines, to predict human drug absorption. For a number of reasons, the in vitro P_{app} values cannot be directly equated to the corresponding in situ P_{eff} values. This has led to some unintended views concerning drug transport in the human intestine.

To better understand the in situ−in vitro relationship (apart from simple statistical correlation), four interrelated topics can be considered: (a) absorption-accessible intestinal surface area,[32−39] (b) in vivo paracellular junctions (capacity factor, pore size/distribution, molecular hydrodynamic radius),[40−45] (c) in vivo aqueous boundary layer resistance (with possible in situ and in vivo differences),[46−52] and (d) in vivo transcellular permeability (passive, carrier/receptor-mediated, and/or active).[53,54]

The anatomical components of the small intestine (particularly the jejunum and ileum) are evolved to absorb a large proportion of the nutrient intake of the GIT.[32,33] The jejunum,[1−3,32−39] Figure 1, consists of circular folds protruding the cell surface into the luminal fluid, enlarging the available absorptive area in the jejunum by about 3-fold, compared to a "smooth tube" model.[55−57] On top of this circularly rumpled inner surface is a secondary surface-expanding feature consisting of the villus "fingers," further increasing the surface by about 10-fold.[34,55−57] Hence, the available mucosal surface in the human jejunum is potentially 30 times the smooth tube surface in area.

In established practice, the in situ P_{eff} values are calculated in terms of the smooth-tube surface area, although it is

†Contribution number 28 in the *Drug Absorption in Vitro Model* series from *p*ION. Reference 58 is part 27 in the series.

*To whom correspondence should be addressed. For A.A.: phone, +1 781 935 8939; fax, +1 781 935 8938; E-mail: aavdeef@pion-inc.com. For K.Y.T.: phone, +44 (0)1625 230338; E-mail: kin.tam@astrazeneca.com.

[a] Abbreviations: Caco-2, human cancer of the colon epithelial cell line; D_{aq}, aqueous diffusivity ($cm^2\ s^{-1}$); $E(\Delta\varphi)$, function due to potential drop across the cell junction, eq 6 (dimensionless); $F(r/R)$, Renkin molecular sieving function (dimensionless fraction, 0−1), eq 4; $f_{(o)}$, $f_{(+)}$, $f_{(-)}$, concentration fraction of the molecule in the uncharged, positively, and negatively charged forms, respectively; h_{ABL}, aqueous boundary layer thickness (cm); k_{VF}, villus-fold surface area expansion factor (dimensionless); MDCK, Madin−Darby canine kidney epithelial cell line; P_{eff}, effective human jejunal permeability coefficient ($cm\ s^{-1}$); P_c, transcellular cell permeability coefficient ($cm\ s^{-1}$); P_{ABL}, aqueous boundary layer permeability coefficient ($cm\ s^{-1}$); P_{para}, paracellular permeability ($cm\ s^{-1}$); P_{OCT}, octanol−water partition coefficient; PAMPA, parallel artificial membrane permeability assay; %F, human absolute bioavailability; %para, relative fraction of transport effected by the paracellular route; %trans, relative fraction of transport effected by the transcellular route; P_{app}, apparent cellular (Caco-2) permeability; r_{HYD}, hydrodynamic molecular radius (Å), eq 5; R, membrane junction pore radius (Å); ε/δ, porosity of paracellular junction pores divided by the rate-limiting paracellular path length (high-capacity, size-restricted, cation-selective); ε/δ_2, secondary porosity-path length ratio (low-capacity, size- and charge-independent); $\Delta\varphi$, potential drop across the electric field created by negatively charged residues lining the junctional pores.

 Published on Web 04/07/2010

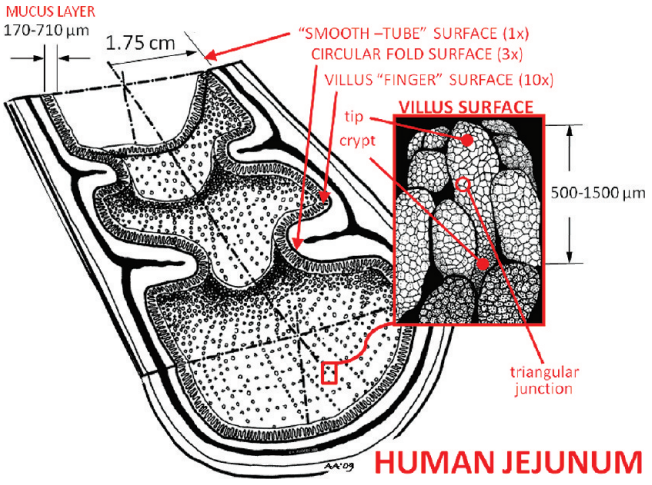

Figure 1. View of cross section of the human jejunum, indicating the circular fold and the villus surface expanding features and some of the dimensions of components.

generally acknowledged by the practitioners that the true surface available for absorption may be larger than indicated by this approximation (Figure 1). On the other hand, the in vitro cell monolayers form smooth flat surfaces when seeded on filters (apart from the microvillus structure, which is common to both the in vitro and in vivo cells). Consequently, the P_{eff} value for a given permeant could be up to 30 times greater than the corresponding Caco-2 P_{app} value.

Although the surface area issue is widely recognized, it is not entirely clear how to incorporate the appropriate scaling to the P_{eff} values. One challenge is that the surface appears not to be equally accessible to all permeants based on rodent data. From studies of anaesthetized rats, the ratio $P_{app}^{Caco\text{-}2}/P_{eff}$ significantly depends on the value of P_{eff}, with ratio values in the rat as low as 0.15 for poorly permeable compound and as high as 0.4 for highly permeable molecules.[35] This can be explained if lipophilic molecules are quickly absorbed at the protruding villus tips (Figure 1), which have the effective surface area near the smooth-tube value, and if hydrophilic molecules (whose absorption is slow and incomplete) are exposed to the whole available mucosal surface, which could be 30 times greater than the smooth tube value (not counting the microvillus contribution). An articulate mathematical model describing the "accessibility factor" for the rat intestine has been published by Oliver et al.[37] The idea of variable accessibility is now widely accepted.[36−38,44−46,59] However, as far as we are able to determine, it still remains to be shown to what extent the accessibility concept applies to *unanaesthetized* human subjects undergoing intestinal perfusion.

The tight junctions between cells are an important protective barrier in the GIT that regulate the diffusion of small polar/ionic solutes through size-restricted and cation-selective water-filled "paracellular" channels but largely exclude potentially toxic large molecules. Adson et al.[43] quantitatively characterized the leakiness and size exclusion properties of the paracellular junctions in Caco-2 monolayers in terms of three parameters: ε/δ (porosity−path length ratio − a capacity factor), R (pore radius), and $\Delta\varphi$ (electrical potential drop in the channels). The porosity, ε, is defined as the area of exposed aqueous channels divided by the total cell surface area exposed to the lumen. Estimates range from 10^{-3} to 10^{-5} for ε.[1,3,41] A capacity factor may be defined by the ratio ε/δ, where δ is the rate-limiting paracellular junction path length.[43,53,58] Values of the capacity factor in the in vitro cellular models range from 0.2 to 69 cm^{-1}, with most values < 1.5 cm^{-1}.[58] Values of ε/δ for the human intestine based on drug molecules have not been reported. Estimates of R span 4−13 Å, mostly based on Caco-2 models.[58] The average paracellular potential drop in Caco-2 models was estimated to be $\Delta\varphi = -43 \pm 20$ mV, drawing on data from several laboratories.[58]

The aqueous boundary layer (ABL) adjacent to epithelial cells includes the 170−710 μm thick continuously secreted mucus layer (Figure 1).[46−52] When solutes enter this stagnant water layer, their further movement is primarily due to aqueous diffusion, with minimal contribution from convection (under isotonic conditions). Vigorous agitation makes the ABL thinner and thus less resistive to solute transport. Under natural in vivo conditions, the undulating motion of the small intestine causes the watery luminal fluid to mix and descend slowly down the GIT. The attendant motion of the villus fingers (Figure 1) is believed to cause the fluid in the intervillus space to be particularly well-mixed.[19,39,50,53] In the fasted in vivo state, the small intestine takes on a flat shape[35] (like a fire-hose drained of water). Naturally, the expected ABL thickness would not be much greater than that of the mucus layer. However, in the in situ perfusion experiment, the distended jejunum swells to a circular cylindrical shape,[31] with the perfusion fluid occupying the nonmucus luminal volume. It may be that a perfusion flow rate of 2 mL min^{-1} in the distended tube is not sufficient to vigorously mix the intestinal fluid segment. But because the human subjects are awake during the perfusion, the natural peristalsis is thought to perform additional mixing, particularly in the intervillus spaces and the adherent mucus layer, as reviewed by Lennernäs.[3] According to the Johnson−Amidon[60] cylindrical-flow equation, applied to a smooth cylinder, the ABL thickness is predicted to be about 2800 μm for a drug molecule with a molecular weight of 300 Da. In the perfusion experiment, therefore, some regions may be well mixed but perhaps not all regions.

To address some of the above complexity, this study describes a novel analysis of the human jejunal permeability data, based on a significant extension of an earlier in vitro model,[58] in terms of the combined effects of (a) the absorption-accessible surface area, (b) a new dual-pore variant of the Adson paracellular model, and (c) the ABL- and paracellular-corrected Caco-2/MDCK values equated to in vivo transcellular permeability. This investigation showed that the unstirred water layer thickness in the human in situ perfusion experiments is much greater than had been commonly thought, the absorption-accessible mucosal surface area in humans is apparently not dependent on lipophilicity of the drug, in contrast to rodent studies, and the relative "leakiness" of the human jejunum is not so different from that observed in a number of Caco-2 studies.

Theoretical Section

Computational Method. Although the refinement model described below may appear complex, its description is complete, and the parameters determined here can be readily adapted to calculate molecular transport properties using very common software programs such as Microsoft Excel.

Model Equation. The model developed here begins with the deconvolution of P_{eff} into its three effective components:

P_{eff}^{ABL}, P_{eff}^{trans}, and P_{eff}^{para} (ABL, transcellular, and paracellular permeability, respectively).[59] It is postulated here that P_{eff}^{trans} in the human jejunum can be modeled using the P_{app} values taken from Caco-2 studies at pH 6.5, provided that the values are adjusted to remove any contributions from the in vitro ABL and the in vitro paracellular permeability (yielding Caco-2 "cell"[54] permeability, $P_c^{6.5}$) and furthermore multiplied by the villus-and-fold surface expansion factor: $P_{eff}^{trans} = k_{VF} \cdot P_c^{6.5}$. For passively permeating molecules, this may be a reasonable assumption. (However, there would be increased uncertainty for actively transported drugs, if the relative levels of expression of the transporters in the in vitro system and the in vivo intestinal environment were not well matched. Carrier protein expression in the GIT was recently reviewed by Lennernäs.[3]) It is further assumed that a somewhat modified (dual pore size) Adson model can be used to frame the P_{eff}^{para} calculation. Lastly, it is assumed that $P_{eff}^{ABL} = k_{VF} \cdot D_{aq}/h_{ABL}$, where D_{aq} is the aqueous diffusivity of the molecule and h_{ABL} is the absolute aqueous boundary layer thickness in the in situ perfusion experiment.

To construct and test the prediction model incorporating the above assumptions, a weighted nonlinear regression method has been developed to determine the parameters, using the human P_{eff} as dependent and the Caco-2 P_{app} (specifically, $P_c^{6.5}$) as independent variables.

$$\frac{1}{P_{eff}} = \left(\frac{1}{P_{eff}^{ABL}} + \frac{1}{P_{eff}^{trans} + P_{eff}^{para}}\right) = \frac{1}{k_{VF}} \cdot \left(\frac{h_{ABL}}{D_{aq}} + \frac{1}{P_c^{6.5} + P_{para}}\right) \quad (1)$$

Values of D_{aq} ($cm^2\ s^{-1}$) at 37 °C were empirically estimated from the molecular weight, MW, as

$$D_{aq} = 0.991 \times 10^{-4} MW^{-0.453} \quad (2)$$

which was derived from the analysis of 147 mostly drug-like molecules (MW < 1200 Da).[58] The thickness of the physical boundary layer, h_{ABL}, depends on the agitation level in the in situ perfusion experiment. With in vitro (microtiter plate) methods, typical values are about 1000−4000 μm in unstirred solutions and about 500 μm in solutions stirred at 50 rpm (rev min^{-1}).[58]

P_{para} can be estimated from the mathematical solution to the differential flux equation describing size- and charge-restricted diffusion through a cylindrical channel containing charged groups under sink boundary condition.[43,53] As a minor extension to the Adson model, it was assumed here that there exist two populations of junctional pores: (a) high-capacity ε/δ, size-restricted and cation-selective pathways, and (b) secondary ε/δ_2 low-capacity, size- and charge-independent pathways. The dual-pore population paracellular equation proposed here is

$$P_{para} = \frac{\varepsilon}{\delta} \cdot D_{aq} \cdot F\left(\frac{r_{HYD}}{R}\right) \cdot E(\Delta\varphi) + \frac{\varepsilon}{\delta_2} \cdot D_{aq} \quad (3)$$

where most of the terms have been defined already. The last term in eq 3 describes the minor secondary pathway contribution ($\varepsilon/\delta > \varepsilon/\delta_2$). $F(r_{HYD}/R)$ is the Renkin hydrodynamic sieving function[53] for cylindrical water channels, with values ranging from 0 to 1, defined as a function of molecular hydrodynamic radii (r_{HYD}) and pore radii (R), both usually expressed in Å units,

$$F\left(\frac{r_{HYD}}{R}\right) = \left[1 - \left(\frac{r_{HYD}}{R}\right)\right]^2 \cdot \left[1 - 2.104\left(\frac{r_{HYD}}{R}\right) + 2.09\left(\frac{r_{HYD}}{R}\right)^3 - 0.95\left(\frac{r_{HYD}}{R}\right)^5\right] \quad (4)$$

The reliability of the equation decreases for $r_{HYD}/R > 0.4$, but the equation may still be useful. Values of r_{HYD} were estimated from the Sutherland−Stokes−Einstein spherical-particle equation,[58]

$$r_{HYD} = \left(0.92 + \frac{21.8}{MW}\right) \cdot r_{SE} \quad (5)$$

where r_{SE} is calculated from the Stokes−Einstein equation: r_{SE} (Å) = $10^{+8}\ k_B T/(6\pi\ \eta\ D_{aq})$; k_B = Boltzmann constant, T = absolute temperature, and η = solvent kinematic viscosity (0.006962 $cm^2\ s^{-1}$, 37 °C). The $E(\Delta\varphi)$ term in eq 3 is a function of the potential drop, $\Delta\varphi$, across the electric field created by negatively charged residues lining the junctional pores, and can be defined as[43,53,58]

$$E(\Delta\varphi) = f_{(0)} + f_{(+)} \cdot \frac{\kappa \cdot |\Delta\varphi|}{1 - e^{-\kappa \cdot |\Delta\varphi|}} + f_{(-)} \cdot \frac{\kappa \cdot |\Delta\varphi|}{e^{+\kappa \cdot |\Delta\varphi|} - 1} \quad (6)$$

where $f_{(o)}$, $f_{(+)}$, and $f_{(-)}$ are the concentration fractions of the molecule in the uncharged, cationic, and anionic forms, respectively. The constant, $\kappa = (F/N_A k_B T) = 0.037414\ mV^{-1}$ at 37 °C, where F is the Faraday constant and other symbols have their usual meaning. The average $\Delta\varphi$ of −43 mV for Caco-2 suggests that a negatively and a positively charged molecule would have P_{para} reduced to 41% and increased to 201%, respectively, of the charge-free value.

Refinement of the Permeability Parameters. The *p*CEL-X v2.3 program (*p*ION) was used to determine the k_{VF}, h_{ABL}, ε/δ, ε/δ_2, R, and $\Delta\varphi$ parameters by a weighted nonlinear regression analysis based on the logarithmic form of eq 1, expanded with eqs 2−6:

$$G\left(k_{VF}, h_{ABL}, \frac{\varepsilon}{\delta}, \frac{\varepsilon}{\delta_2}, R, \Delta\varphi\right) = \log k_{VF} - \log\left[\frac{h_{ABL}}{D_{aq}} + \frac{1}{P_c^{6.5} + \frac{\varepsilon}{\delta} \cdot D_{aq} \cdot F\left(\frac{r_{HYD}}{R}\right) \cdot E(\Delta\varphi) + \frac{\varepsilon}{\delta_2} \cdot D_{aq}}\right] \quad (7)$$

The partial derivatives of G with respect to ε/δ, ε/δ_2, R, $\Delta\varphi$, h_{ABL}, and k_{VF} are calculated explicitly in the *p*CEL-X program based on standard mathematical techniques. The weighted residuals function minimized was

$$R_w = \sum_i^n \left(\frac{\log P_{eff,i}^{obsd} - G_i^{calcd}}{\sigma_i(\log P_{eff})}\right)^2 \quad (8)$$

where n is the number of P_{eff} values used in the model refinement (maximum of 119), and $\sigma_i(\log P_{eff})$ is the reported standard deviation of the logarithm of the ith measured human jejunal permeability. The effectiveness of the refinement was characterized by the "goodness-of-fit", GOF = $[R_w/(n - n_V)]^{1/2}$, where n_V refers to the number of varied parameters (maximum of 6). The expected value of GOF is 1

Table 1. Absorption, Physicochemical, and Cell Permeation Properties of Compounds [a]

compd	%*F*	MW	log P_{OCT}	pK_a	*f*(0)	*f*(+)	*f*(−)	predominant charge	D_{aq} (10^{-6} cm^2 s^{-1})	r_{HYD} (Å)	log $P_c^{6.5}$ Caco-2/MDCK	refs
acetaminophen	85 ± 4	151.2	0.34	9.63	1.00	0.00	0.00	0	10.2	3.4	−4.04 ± 0.51	62, 96
α-methyl-DOPA	26 ± 14	211.2	−3.00	8.94 2.21	1.00	0.00	0.00	±	8.8	3.8	−6.40	63
amiloride	50 ± 10	229.6	−0.26	10.19 8.65	0.01	0.99	0.00	+	8.4	3.9	−6.72 ± 0.28	64, 65
amoxicillin	45−75	365.4	−1.71	7.0 2.6	0.76	0.00	0.24	±,−	6.8	4.7	−5.79 ± 0.04	64, 66
antipyrine	99 ± 1	188.2	0.56	*1.3*	1.00	0.00	0.00	0	9.2	3.7	−3.91 ± 0.24	64, 65, 67−69, 96
atenolol	50−60	266.3	0.22	9.19	0.00	1.00	0.00	+	7.9	4.2	−7.04 ± 0.34	62, 64, 66, 70−73, 96
benserazide	70	257.2	*−1.78*	7.97 6.19	0.66	0.32	0.02	0,+	8.0	4.1	−4.90 ± 0.34	64
carbamazepine	90−100	236.3	2.45		1.00	0.00	0.00	0	8.3	4.0	−3.14 ± 0.57	64, 66
cephalexin	90−100	347.4	−0.47	7.05 2.55	0.78	0.00	0.22	±,−	7.0	4.6	−6.14 ± 0.05	62, 74, 96
cimetidine	60 ± 7	252.3	0.48	6.76	0.35	0.65	0.00	+,0	8.1	4.1	−6.27 ± 0.30	65, 66, 69, 75−78
creatinine	80	113.1	−3.00	4.66	0.99	0.01	0.00	0	11.6	3.1	−6.01 ± 0.14	64, 79
cyclosporine A	44 ± 14	1202.6	3.54		1.00	0.00	0.00	0	4.0	7.7	−5.16 ± 0.16	65, 69
desipramine	70 ± 8	266.4	3.79	9.80	0.00	1.00	0.00	+	7.9	4.2	−5.05 ± 0.22	64, 65
D-glucose	100	180.2	−0.67		1.00	0.00	0.00	0	9.4	3.6	−4.68 ± 0.11	19, 80
enalapril	51 ± 6	376.5	*−1.39*	5.57 2.92	0.11	0.00	0.89	−, ±	6.7	4.7	−5.66 ± 0.11	19, 80
enalaprilat	8	348.4	−0.13	*7.6* *3.2*	0.00	0.00	1.00	−	7.0	4.6	−8.81 ± 0.34	64
fexofenadine	30 ± 3	501.7	*2.08*	7.84 4.20	0.95	0.00	0.04	±	5.9	5.3	−6.32 ± 0.66	81, 82
fluvastatin	95	411.5	4.17	4.31	0.01	0.00	0.99	−	6.5	4.9	−3.57 ± 0.01	65
furosemide	40−60	330.8	2.56	9.87 3.51	0.00	0.00	1.00	−	7.1	4.5	−6.54 ± 0.78	64, 71, 75, 83, 84, 96
griseofulvin	95 ± 5	352.8	2.18		1.00	0.00	0.00	0	6.9	4.6	−4.44 ± 0.33	85
hydrochlorothiazide	55 ± 9	297.7	−0.03	9.78 8.53	0.99	0.00	0.01	0	7.5	4.3	−6.28 ± 0.22	62, 64, 66, 71, 86, 96
inogatran	5−10	438.6	*−0.60*	7.6 1.6	0.93	0.00	0.07	±	6.3	5.0	−7.2 [c]	
ketoprofen	100	254.3	3.16	4.02	0.00	0.00	1.00	−	8.0	4.1	−3.75 ± 0.09	62, 64, 66−68
L-DOPA	100	197.2	−3.00	8.54 2.21	0.99	0.00	0.01	±	9.0	3.7	−5.94 ± 0.45	69
lisinopril	27 ± 3	405.5	−2.86	7.01 3.16	0.76	0.00	0.24	±,−	6.5	4.9	−5.85 ± 0.56	64, 66
L-leucine	100	131.2	−1.55	9.61 2.38	1.00	0.00	0.00	±	10.9	3.3	−4.90 ± 0.47	64, 69
losartan	50 ± 13	422.9	*3.74*	4.25 2.95	0.01	0.00	0.99	−	6.4	5.0	−5.62 ± 0.34	87
L-phenylalanine	100	165.2	−1.38	8.92 2.20	1.00	0.00	0.00	±	9.8	3.5	−4.63 ± 0.34	64
metoprolol	95	267.4	1.95	9.18	0.00	1.00	0.00	+	7.9	4.2	−4.70 ± 0.43	64−66, 68, 73, 88, 89
naproxen	100	230.3	3.24	4.00	0.00	0.00	1.00	−	8.4	3.9	−3.33 ± 0.25	64−67, 75
PEG238		238.3	−2.21		1.00	0.00	0.00	0	8.3 [f]	4.0 [f]	−5.37 [b]	61
PEG282	79	282.3	*−2.54*		1.00	0.00	0.00	0	7.7 [f]	4.2 [f]	−5.62 [b]	61
PEG326	71	326.4	*−2.76*		1.00	0.00	0.00	0	7.2 [f]	4.5 [f]	−6.20 [b]	61
PEG370	48	370.4	−3.08		1.00	0.00	0.00	0	6.8 [f]	4.7 [f]	−6.76 [b]	61
PEG414	29	414.5	*−3.12*		1.00	0.00	0.00	0	6.5 [f]	4.9 [f]	−7.24 [b]	61
PEG458	18	458.5	*−3.27*		1.00	0.00	0.00	0	6.2 [f]	5.1 [f]	−7.31 [b]	61
PEG502	11	502.6	−3.40		1.00	0.00	0.00	0	5.9 [f]	5.3 [f]	−7.26 [b]	61
PEG546	3−7	546.6	*−3.53*		1.00	0.00	0.00	0	5.7 [f]	5.5 [f]	−7.31 [d]	
PEG590	2.4	590.7	*−3.65*		1.00	0.00	0.00	0	5.5 [f]	5.7 [f]	−7.31 [d]	
PEG810	1.1	810.9	*−4.13*		1.00	0.00	0.00	0	4.8 [f]	6.5 [f]	−7.31 [d]	
PEG942	1.0	943.1	*−4.35*		1.00	0.00	0.00	0	4.4 [f]	6.9 [f]	−7.31 [d]	
piroxicam	100	331.4	1.98	5.34 1.88	0.06	0.00	0.94	−	7.1	4.5	−3.60 ± 0.34	64
propranolol	100	259.3	3.48	9.17	0.00	1.00	0.00	+	8.0	4.1	−4.46 ± 0.39	64−68, 72, 73, 75, 88, 89
quercetin-3, 4′-diglucoside	60 ± 31	464.4	3.24	9.4 6.9	0.71	0.00	0.28	0,−	6.1	5.2	−6.7 [c]	
ranitidine	50−60	314.4	1.28	8.00 2.11	0.03	0.97	0.00	+	7.3	4.4	−8.90 ± 0.34	90

Table 1. Continued

compd	%*F*	MW	log P_{OCT}	pK_a	*f*(0)	*f*(+)	*f*(−)	predominant charge	D_{aq} (10^{-6} cm^2 s^{-1})	r_{HYD} (Å)	log $P_c^{6.5}$ Caco-2/MDCK	refs
retinoic acid	90	300.4	6.30	4.52	0.01	0.00	0.99	−	7.5	4.3	−2.84 ± 0.03	this work
salicylic acid	100	138.1	2.19	2.88	0.00	0.00	1.00	−	10.6	3.3	−4.12 ± 0.24	62, 75, 89, 91, 92, 96
sulforaphane	74 ± 29	177.3	*1.68*		1.00	0.00	0.00	0	9.5	3.6	−3.85 ± 0.04	this work
terbutaline	14 ± 5	225.3	−0.08	9.97 8.67	0.01	0.99	0.00	+	8.5	3.9	−7.26 ± 0.80	64, 65, 96
urea		60.1	−1.64		1.00	0.00	0.00	0	15.5	2.7	−6.05 ± 0.26 [e]	93
valacyclovir	80−100	324.3	*−1.04*	9.23 7.40	0.11	0.89	0.00	+,0	7.2	4.5	−5.83 ± 0.34	94
verapamil	84 ± 4	454.6	4.33	8.76	0.01	0.99	0.00	+	6.2	5.1	−4.57 ± 0.50	54, 64−67, 69, 83, 88
water		18.0			1.00	0.00	0.00	0	26.7	2.6	−6.0 [e]	95

[a] The absolute bioavailability, %*F*, data for drug molecules were taken from refs 3, 30, 105, 112, 116, 117, and have been corrected for first pass hepatic clearance as appropriate; while for PEGs the %F data were from refs 17 and 110. pK_a and log P_{OCT} (octanol−water partition coefficient) were taken from various standard sources.[36,97,98] $f_{(0)}$, $f_{(+)}$, and $f_{(-)}$ refer to concentration fractions of the compound at pH 6.5 in the neutral, cationic and anion forms, respectively. log $P_c^{6.5}$ is the average value of the charge-, ABL-, and paracellular-corrected Caco-2/MDCK log P_{app} value. Aqueous diffusivity, D_{aq}, calculated by eq 2; molecular hydrodynamic radius, r_{HYD}, calculated by eq 5. [b] Untreated log P_{app} values; see Table 5 for lop P_c values. [c] Calculated by pCEL-X because reliable literature values were not found. [d] Approximated, based on measured PEG458 value. [e] Approximate value based on rat in situ brain perfusion data. [f] Not used; see Table 5 for D_{aq} values used in refinement.

if the model is suitable for the data and the measured standard deviations accurately reflect the precision of the data.

Effective Human Jejunal Permeability Data Sources. Human permeability data for 53 drug and test compounds (119 P_{eff} values) have been published in the open literature.[3−31] Table 1 lists the physical properties of the molecules; their structures are shown in Figure 2. By far, most of the data originate from the laboratories of Profs. Hans Lennernäs (Uppsala University) and Gordon Amidon (University of Michigan).[7,8,12−31] Earlier investigators, using the open single-pass jejunal perfusion method, published data in terms of absorption, e.g., in μg min^{-1} (30 cm)$^{-1}$ units.[5,9−11] These quantities were converted to P_{eff} values by dividing by the surface area of the segment (assuming 1.75 cm intestinal radius) and then by the permeant concentration in the perfusate. Of the two dosing values given in the acetaminophen study,[10] 250 μg mL^{-1} was used. For the range of absorption values given for ranitidine, the lowest value, 160 μg min^{-1} (30 cm)$^{-1}$ was used. The Chadwick et al.[4] human intestinal absorption data for polyethylene glycols were converted to the P_{eff} scale by Artursson et al.,[61] whose values were used here. The Sutcliffe et al.[6] data for five drugs were reported as %lost. These values were transformed as: $P_{eff} = -Q\cdot(2\pi\cdot R\cdot L\cdot 60)^{-1}\ln(1 - \%\text{lost}/100)$, where $R = 1.75$ cm, $L = 30$ cm, and Q is the perfusion flow velocity (cm^3 min^{-1}). Table 2 lists the collated P_{eff} data used in this study. We were not successful in locating the standard deviations for a number of the compounds in Table 2. Consequently, in the regression model, the missing values were set to the average of the reported standard deviations.

In Vitro Data Used to Approximate Effective Jejunal Transcellular Permeability. For the compounds whose human jejunal permeability coefficients were reported, the corresponding in vitro P_{app} values were obtained from the literature, except for sulforaphane, retinoic acid, inogatran, and quercetin-3,4′-diglucoside. To fill in some of the missing data, the Caco-2 P_{app} coefficients of sulforaphane and retinoic acid were determined in this study. Because a commercial source for inogatran and quercetin-3,4′-diglucoside was not located, these two remaining missing P_{app} values were calculated, using the Caco-2 database in the *p*CEL-X program. Table 1 lists the reduced Caco-2 data used in the study. Specifically, the P_{app} values reported in the literature[60−95] for the molecules studied were converted to the $P_c^{6.5}$ scale, after calculating out the in vitro paracellular and in vitro aqueous boundary layer contributions from the apparent permeability values, then making any necessary pH adjustments, according to the procedure described in detail elsewhere,[53,54] using the *p*CEL-X computer program.

As the in vitro data were assembled, it was found that many molecules were characterized both with Caco-2 and MDCK models. The former is a human colon cell line, whereas the latter is a canine kidney cell line. Both are popular in pharmaceutical research. There are some important differences between the two epithelial cell lines. For example, the expression of some transporters in the MDCK cells is attenuated, compared to that in Caco-2.[62,65,66,69,70,78,81,84] Nevertheless, we were interested to see if the cell permeability values derived from the two systems were comparable. Figure 3 shows a plot of the intrinsic permeability values, log P_o (permeability of the uncharged form of the molecule[54,97]), for the two cellular models for 79 compounds (mostly passive transcellular type). Statistically, the two models are comparable, as indicated by the metrics in Figure 3. Consequently, the data from the two cell lines were merged for the purpose of calculating the mean values for use in modeling P_{eff}.

Most of the reported studies from which the Caco-2 or MDCK values were taken also contained data for paracellular marker molecules, e.g., mannitol or urea. These were used to remove the paracellular contribution to the apparent data.[58] The extent of the contribution of the aqueous boundary layer was estimated by predicting P_{ABL} (using the *p*CEL-X program), using the reported stirring conditions. P_{app} values for test compounds near the predicted P_{ABL} limit were avoided due to the uncertainty of the correction required to remove the ABL component. We avoided data for very lipophilic compounds reported in studies where stirring was not employed. In studies where vigorous stirring was employed, the contribution due to the ABL resistance was small for all but the most lipophilic molecules. If the measured Caco-2/MDCK data were reported at several different values of pH,[54,64,66−68,72,74−76,83,91,96] it was possible to directly calculate out the ABL and paracellular contributions to P_{app}, following the procedure described elsewhere.[54]

It was a challenge to estimate the Caco-2 $P_c^{6.5}$ values of molecules that are themselves paracellular markers, e.g., water, urea, creatinine, and polyethylene glycols. For water and urea,

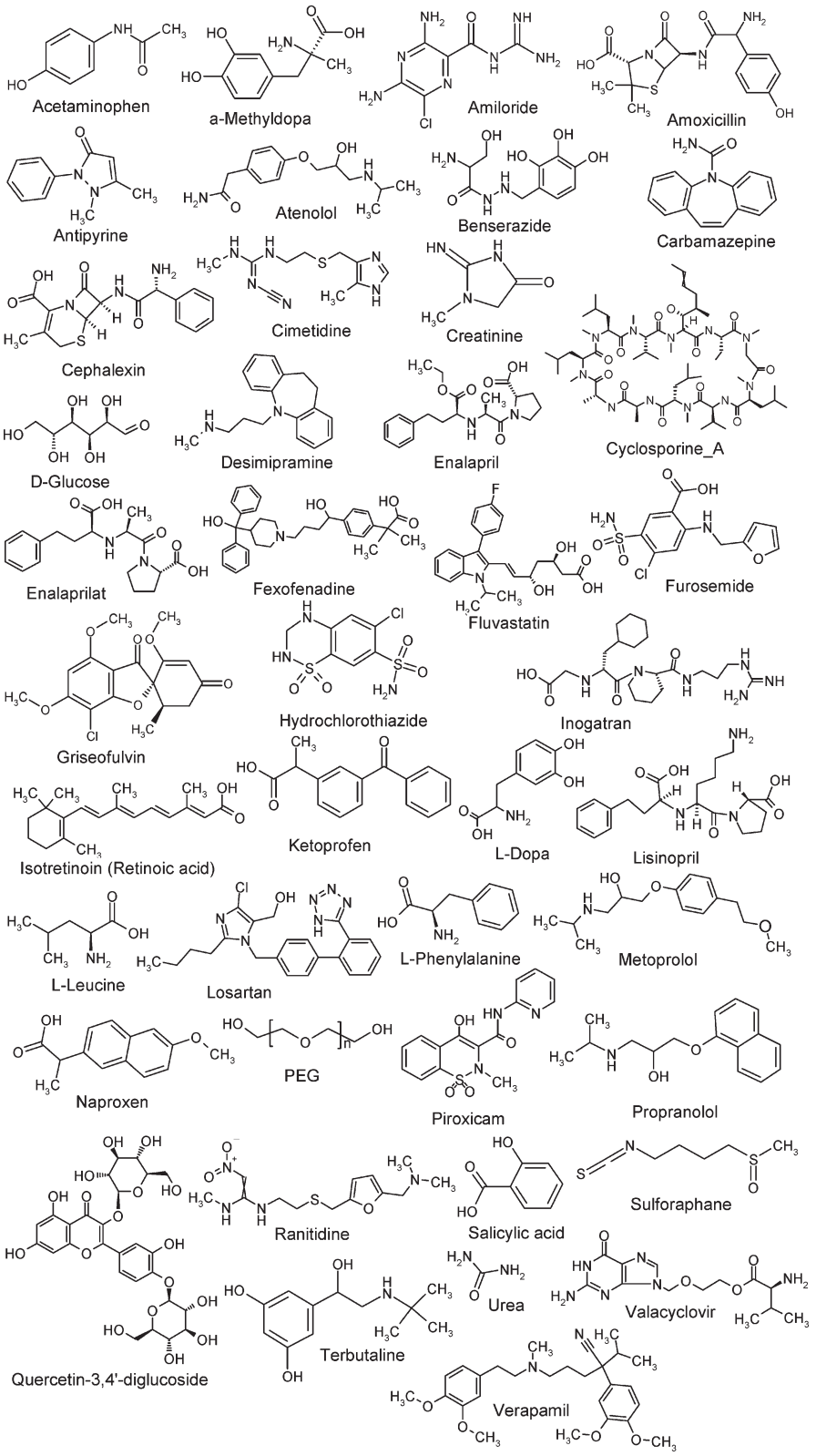

Figure 2. Structures of the compounds whose human jejunal permeability values have been determined by the regional single-pass perfusion technique.

we used permeability values taken from published in situ brain perfusion data[93,95] (cf. Table 1), where the paracellular junctions are thought to be very tight for such hydrophilic molecules. For the paracellular-marker PEG series of molecules, we deduced values of P_c[6.5] using a procedure that is an extension of what had been described elsewhere.[58]

Results and Discussion

Caco-2 Permeability of Sulforaphane and Retinoic Acid. Figure 4 shows the log P_{app} vs pH profile for retinoic acid. The circle symbols indicate the five measured P_{app} values in the gradient pH 6.0−8.0 range. The solid P_{app} curve is the

Table 2. Effective Human Jejunal Permeation Data

compd	P_{eff} 10^{-4} cm s^{-1}	refs	compd	P_{eff}(human),10^{-4} cm s^{-1}	refs
acetaminophen	1.76 ± 0.43	10	ketoprofen	8.4 ± 3.3	20
α-methyl-DOPA	0.1 ± 0.1	8		8.5 ± 3.9	14
	0.2 ± 0.06	20	L-DOPA	3.4 ± 1.0	8
amiloride	1.63 ± 0.51	24		3.4 ± 1.7	19
amoxicillin	0.3 ± 0.4	20		3.41 ± 2.59	8
	0.34 ± 0.11	24	lisinopril	**0.33** [a]	3
antipyrine	2.07 ± 1.41	15	L-leucine	6.20 ± 2.93	8
	3.96 ± 1.33	31	losartan	1.14 ± 1.1	27
	4.05 ± 1.08	24	L-phenylalanine	3.36 ± 2.74	23
	4.5 ± 2.5	20		**4.08** [a]	3
	4.6 ± 2.8	21		4.31 ± 2.11	18
	5.02 ± 1.61	22		4.54 ± 2.39	29
	5.3 ± 2.5	7	metoprolol	0.90 ± 0.08	5
	5.6 ± 1.6	19		0.92 ± 0.39	15
	5.7 ± 3.0	12		1.2 ± 0.9	19
	6.0 ± 2.0	13		1.3 ± 1.0	20
	7.3 ± 3.8	30		1.5 ± 0.9	16
	8.36 ± 4.81	8	naproxen	8.0 ± 4.2	14
atenolol	0.12 ± 0.2	19		8.3 ± 4.8	20
	0.14 ± 0.18	12		**8.5** [a]	3
	0.15 ± 0.2	16		10.0 ± 4.7	19
	0.2 ± 0.2	20		10.0 ± 3.7	16
	0.27 ± 0.2	15	PEG238	5.18 ± 0.02	4, 60
	0.38 ± 0.10	6	PEG282	4.34 ± 0.03	4, 60
benserazide	2.9 ± 1.3	8	PEG326	3.01 ± 0.04	4, 60
carbamazepine	4.3 ± 2.7	20	PEG370	2.63 ± 0.05	4, 60
cephalexin	**1.56** [a]	3	PEG400	0.555 ± 0.381	18
cimetidine	**0.26** [a]	3		0.559 ± 0.446	23
	0.299 ± 0.157	23		0.83 ± 0.51	29
	0.77 ± 0.34	6	PEG414	1.79 ± 0.07	14
creatinine	0.29 ± 0.16	21	PEG458	1.18 ± 0.11	4, 60
	0.3 ± 0.2	20	PEG502	0.93 ± 0.14	4, 60
cyclosporine A	**1.61** [a]	3	PEG546	0.76 ± 0.17	4, 60
	1.65 ± 0.53	29		1.62 ± 0.75	17
desipramine	4.4 ± 1.8	20	PEG590	0.53 ± 0.24	4, 60
	4.5 [a]	3	PEG810	0.95 ± 0.59	17
D-glucose	5.6 ± 11	21	PEG942	0.97 ± 0.54	17
	6.59 ± 2.94	22	piroxicam	**6.65** [a]	3
	7.2 ± 5.7	13		6.738 ± 3.933	18
	8.8 ± 4.4	7		7.8 ± 7.5	20
	10.0 ± 8.2	20	propranolol	2.698 ± 1.192	18
	18.4 ± 15.2	8		2.8 ± 1.3	16
enalapril	**1.57** [a]	3		2.90 ± 1.28	29
enalaprilat	0.1 ± 0.3	16		2.9 ± 2.2	20
	0.2 ± 0.3	20		3.878 ± 3.940	23
	0.3 ± 0.3	12	quercetin-3,4′-glucoside	8.9 ± 7.1	30
fexofenadine	0.06 ± 0.07	28	ranitidine	0.273 ± 0.247	23
	0.07 [a]	3		**0.47** [a]	9
	0.11 ± 0.11	26	salicylic acid	2.67 ± 0.14	6
fluvastatin	2.38 ± 1.85	15	sulforaphane	18.7 ± 12.6	30
furosemide	0.05 ± 0.04	20	terbutaline	0.3 ± 0.3	13
	0.17 ± 0.07	31	urea	1.4 ± 0.49	21
	0.30 ± 0.30	14		1.4 ± 0.4	20
	0.48 ± 0.13	6	valacyclovir	**1.66** [a]	3
griseofulvin	1.14 ± 0.45	11	verapamil	6.7 ± 2.9	20
hydrochlorothiazide	0.04 ± 0.05	20	verapamil-R	5.56 ± 1.97	22
	0.19 ± 0.11	6		**6.8** [a]	3
inogatran	0.03 ± 0.03	19	verapamil-S	5.62 ± 2.05	22
retinoic acid	**0.99** [a]	3		**6.8** [a]	3
			water	1.4 ± 0.49	21

[a] Standard deviations not available in the cited publication. The average value from all the published standard deviations was applied to these compounds during refinement.

best-fit of the individual points. The dash−dot−dot curve represents the calculated paracellular permeability curve.[58] The upper dotted curve represents the expected ABL permeability, calculated from D_{aq}/h_{ABL}; the diffusivity was estimated by eq 2 and the $h_{ABL} = 156$ μm, corresponding to 384 rpm stirring (*p*CEL-X). However, the lower ABL permeability dotted curve fits the actual data and suggests a high molecular weight diffusing species. A plausible explanation of

the difference between the two ABL curves may be that retinoic acid forms micelles in neutral and acidic solutions. The dashed curve represents the cellular permeability, P_c. This curve is calculated by removing the ABL and the paracellular components from the apparent permeability curve.[58] The top of the P_c curve defines the "intrinsic" permeability, P_o, which indicates the permeability of the uncharged form of retinoic acid. The sparingly soluble uncharged monomeric retinoic acid is an extremely permeable drug, with $P_o = 0.14\ (\pm 0.01)$ cm s^{-1}, but in neutral aqueous solution, its transport appears to be severely limited in the aqueous boundary layer by the putative micelles. The average cell retention, R_{cell}, was 0.54 ± 0.12 (0.33−0.64 range). That is, "mass balance" was 46%. The nonlinear P_{app} equation (eq 10) used in this study compensates for such loss of permeant.[97]

The Caco-2 cellular permeability of sulforaphane was determined to be $P_c = 1.41(\pm 0.13) \times 10^{-4}$ cm s^{-1}. This value represents a 70% transcellular and a 21% ABL contributions to transport, given that the predicted ABL and paracellular permeability values are 4.79×10^{-4} cm s^{-1} and 1.3×10^{-6} cm s^{-1}, respectively. The average cell retention fraction, R_{cell}, was 0.35 ± 0.16, indicating a "mass balance" of 65%.

For the paracellular marker atenolol, $P_{app} = 1.3 \times 10^{-6}$ cm s^{-1} at pH 5.5, which was acceptable for the protocol used.

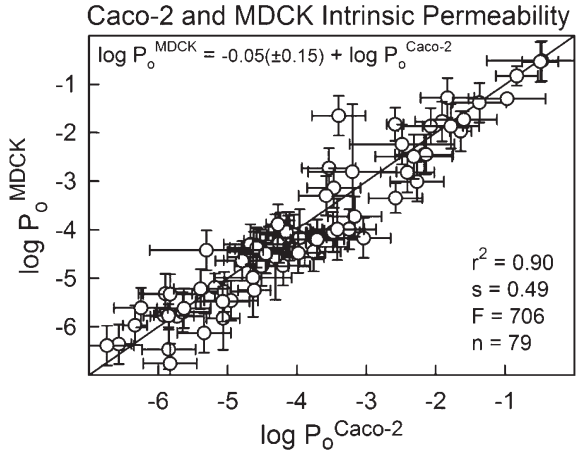

Figure 3. Correlation between the intrinsic permeability determined with the MDCK and the Caco-2 cell lines.

Biophysical Model Regression Analysis. In the course of processing the human P_{eff} data, certain compounds were identified as outliers, in some cases leading to unstable regression. In particular, the entire PEG series showed substantially higher permeability than that predicted by the regression model applied to all 119 P_{eff} values. Additional outliers were L-DOPA, cephalexin, and quercetin-3,4′-diglucoside. In the case of the latter flavonoid molecule, we were not able to find a published Caco-2/MDCK P_{app} value and thus had to rely on the *p*CEL-X predicted value. Because the

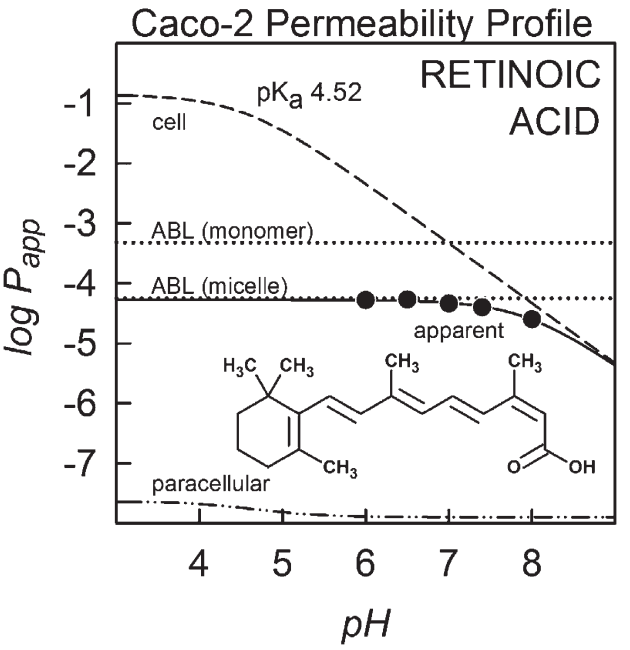

Figure 4. Caco-2 gradient-pH profile data for retinoic acid. The circle symbols indicate the five measured P_{app} values in the pH 6.0−8.0 range. The solid P_{app} curve is the best-fit of the individual points. The dash−dot−dot curve represents the calculated paracellular permeability curve.[58] The upper dotted curve represents the expected ABL permeability, calculated from D_{aq}/h_{ABL}. However, the lower ABL permeability dotted curve fits the actual data and suggests a high molecular weight diffusing species. The dashed curve represents the cellular permeability, P_c. The top of the P_c curve defines the "intrinsic" permeability, P_o, which indicates the permeability of the uncharged form of retinoic acid.

Table 3. Refined Parameters [a]

parameters	Caco-2 (PEG)	Caco-2 (PEG)	human jejunal (PEG)	human jejunal (drugs)
k_{VF}	1 [b]	1 [b]	33.5 [b]	33.5 ± 9.8
R (Å)	4.5 ± 0.1	4.5 ± 0.1	8.2 ± 1.1	11.2 ± 1.7
ε/δ (cm^{-1})	126 ± 11	60 ± 4	15 ± 7	0.53 ± 0.51
ε/δ_2 (cm^{-1})	0.007 ± 0.001	0.013 ± 0.001	0.52 ± 0.72	0.027 ± 0.047
$\Delta\varphi$ (mV)	−30.6 [b]	−30.6 [b]	−30.6 [b]	−30.6 ± 15.8
h_{ABL} (μm)	1500 [b]	1500 [b]	4675 [b]	4675 ± 1812
GOF	1.3	1.1	0.8	1.3
n	7	6	15	99
P_{para} (urea)	33	16	47	3.3
P_{para} (mannitol)	3.1	1.6	15	1.3
P_{para} (sucrose)	0.061	0.099	6.5	0.63
P_{para} (raffinose)	0.042	0.079	4.1	0.38
P_{para}(urea)/P_{app}(raffinose)	786	203	11	9
refs	61	101	4, 17, 18, 23, 29, 61	3−31

[a] R = junction pore radius; k_{VF} = villus-fold surface area expansion factor; ε/δ = porosity/path length junction size-restrictive capacity factor; ε/δ_2 = size-unrestricted secondary pore capacity factor; $\Delta\varphi$ = voltage drop across the paracellular junction; h_{ABL} = physical thickness of the aqueous boundary layer; GOF = goodness-of-fit; n = number of dependent variables considered in refinement; P_{para} = calculated paracellular permeability of markers, based on the refined parameters (in units of 10^{-6} cm s^{-1}). [b] Kept fixed during refinement.

Table 4. Refinement Results [a]

compd	log P_{eff}^{obsd}	SD	log P_{eff}^{calcd}	(obsd−calcd)/SD
acetaminophen	−3.75	0.29	−3.23	−1.79
α-methyl-DOPA	−4.70	0.13	−4.37	**−2.54**
	−5.00	0.43	−4.37	−1.47
amiloride	−3.79	0.14	−4.33	**3.86**
amoxicillin	−4.47	0.14	−4.21	−1.86
	−4.52	0.58	−4.21	−0.53
antipyrine	−3.08	0.25	−3.24	0.64
	−3.14	0.23	−3.24	0.43
	−3.22	0.14	−3.24	0.14
	−3.24	0.23	−3.24	0.00
	−3.25	0.12	−3.24	−0.08
	−3.28	0.20	−3.24	−0.20
	−3.30	0.14	−3.24	−0.43
	−3.34	0.26	−3.24	−0.38
	−3.35	0.24	−3.24	−0.46
	−3.39	0.12	−3.24	−1.25
	−3.40	0.15	−3.24	−1.07
	−3.68	0.30	−3.24	−1.47
atenolol	−4.43	0.11	−4.43	0.00
	−4.57	0.32	−4.43	−0.44
	−4.70	0.43	−4.43	−0.63
	−4.82	0.58	−4.43	−0.67
	−4.85	0.56	−4.43	−0.75
	−4.92	0.72	−4.43	−0.68
benserazide	−3.54	0.19	−3.60	0.32
carbamazepine	−3.37	0.27	−3.24	−0.48
cephalexin	−3.81	*	−4.42	(0.6)
cimetidine	−4.11	0.19	−4.32	1.11
	−4.52	0.23	−4.32	−0.87
	−4.59	0.29	−4.32	−0.93
creatinine	−4.52	0.29	−4.08	−1.52
	−4.54	0.24	−4.08	−1.92
cyclosporine A	−3.78	0.14	−3.89	0.79
	−3.79	0.29	−3.89	0.34
desipramine	−3.35	0.29	−3.68	1.14
	−3.36	0.18	−3.68	1.78
D-glucose	−2.74	0.36	−3.45	**1.97**
	−3.00	0.36	−3.45	1.25
	−3.06	0.22	−3.45	1.77
	−3.14	0.34	−3.45	0.91
	−3.18	0.19	−3.45	1.42
	−3.25	0.85	−3.45	0.24
enalapril	−3.80	0.29	−4.14	1.17
enalaprilat	−4.52	0.43	−4.91	0.91
	−4.70	0.65	−4.91	0.32
	−5.00	1.30	−4.91	−0.07
fexofenadine	−4.96	0.43	−4.59	−0.86
	−5.15	0.29	−4.59	−1.93
	−5.22	0.51	−4.59	−1.24
fluvastatin	−3.62	0.34	−3.36	−0.76
furosemide	−4.32	0.11	−4.66	**3.09**
	−4.52	0.43	−4.66	0.33
	−4.77	0.18	−4.66	−0.61
	−5.30	0.35	−4.66	−1.83
griseofulvin	−3.94	0.29	−3.45	−1.69
hydrochlorothiazide	−4.73	0.27	−4.44	−1.07
	−5.40	0.54	−4.44	−1.78
inogatran	−5.52	0.43	−4.83	−1.60
ketoprofen	−3.07	0.20	−3.28	1.05
	−3.08	0.17	−3.28	1.18
L-DOPA	−3.47	*	−4.18	(0.7)
	−3.47	*	−4.18	(0.7)
	−3.47	*	−4.18	(0.7)
lisinopril	−4.48	0.29	−4.27	−0.72
L-leucine	−3.21	0.21	−3.53	1.52
losartran	−3.94	0.42	−4.12	0.43
L-phenylalanine	−3.34	0.23	−3.42	0.35
	−3.37	0.21	−3.42	0.24
	−3.39	0.29	−3.42	0.10
	−3.47	0.35	−3.42	−0.14
metoprolol	−3.82	0.26	−3.50	−1.23
	−3.89	0.33	−3.50	−1.18
	−3.92	0.33	−3.50	−1.27
	−4.04	0.18	−3.50	**−3.00**
	−4.05	0.29	−3.50	−1.90
naproxen	−3.00	0.20	−3.24	1.20
	−3.00	0.16	−3.24	1.50
	−3.07	0.29	−3.24	0.59
	−3.08	0.25	−3.24	0.64
	−3.10	0.23	−3.24	0.61
PEG238	−3.29	*	−4.56	(1.3)
PEG282	−3.36	*	−4.65	(1.3)
PEG326	−3.52	*	−4.72	(1.2)
PEG370	−3.58	*	−4.79	(1.2)
PEG400	−4.08	*	−4.85	(0.8)
	−4.25	*	−4.85	(0.6)
	−4.26	*	−4.85	(0.6)
PEG414	−3.75	*	−4.85	(1.1)
PEG458	−3.93	*	−4.91	(1.0)
PEG502	−4.03	*	−4.96	(0.9)
PEG546	−3.79	*	−5.01	(1.2)
	−4.12	*	−5.01	(0.9)
PEG590	−4.28	*	−5.05	(0.8)
PEG810	−4.02	*	−5.21	(1.2)
PEG942	−4.01	*	−5.28	(1.3)
piroxicam	−3.11	0.42	−3.32	0.50
	−3.17	0.25	−3.32	0.60
	−3.18	0.29	−3.32	0.48
propranolol	−3.41	0.44	−3.41	0.00
	−3.54	0.19	−3.41	−0.68
	−3.54	0.33	−3.41	−0.39
	−3.55	0.20	−3.41	−0.70
	−3.57	0.19	−3.41	−0.84
quercetin-3,4′-glucoside	−3.05	*	−4.74	(1.7)
ranitidine	−4.33	0.29	−4.55	0.76
	−4.56	0.39	−4.55	−0.03
retinoic acid	−4.00	0.29	−3.28	**−2.48**
salicylic acid	−3.57	0.10	−3.23	**−3.40**
sulforaphane	−2.73	0.29	−3.23	1.72
terbutaline	−4.52	0.43	−4.36	−0.37
urea	−3.85	0.15	−3.95	0.67
	−3.85	0.12	−3.95	0.83
valacyclovir	−3.78	0.29	−4.17	1.34
verapamil	−3.17	0.19	−3.52	1.84
verapamil(R)	−3.17	0.29	−3.52	1.21
	−3.25	0.15	−3.52	1.80
verapamil(S)	−3.17	0.29	−3.52	1.21
	−3.25	0.16	−3.52	1.69
water	−3.85	0.15	−3.73	−0.80

[a] The SD entries marked with * denote points not used in the refinement (zero-weighted). The weighted residuals, (obsd−calcd)/SD, in parentheses, corresponding to the * points, refer to unweighted residuals. Weighted residuals below −2 or above +2 are denoted in bold.

training set data in the computer program does not cover many compounds of this kind, the prediction may be an underestimate. In the final stages of the regression analysis, the P_{eff} data for these outlier molecules, including the PEGs, were assigned zero weights, and the refinement model focused on the "drug subset" of 99 of the 119 P_{eff} values.

The refined parameters from the analysis of the P_{eff} data using eq 7 are summarized in Table 3 (last column).

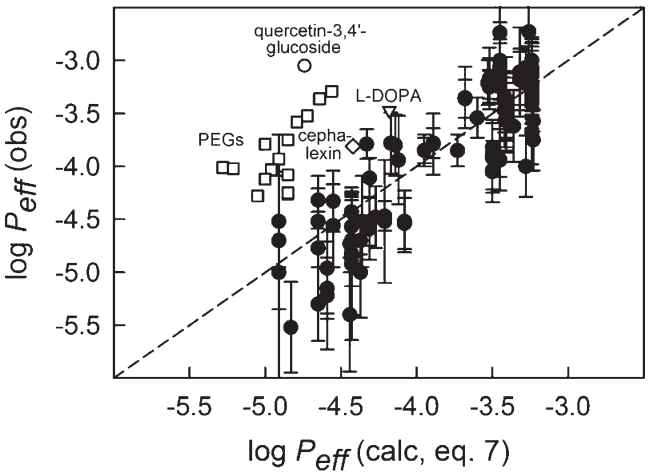

Figure 5. The plot of observed vs calculated log P_{eff}. The zero-weighted PEG P_{eff} data (unfilled symbols) showed consistently high positive residuals, 0.6 −1.3 log units. The other outliers are indicated with unfilled symbols.

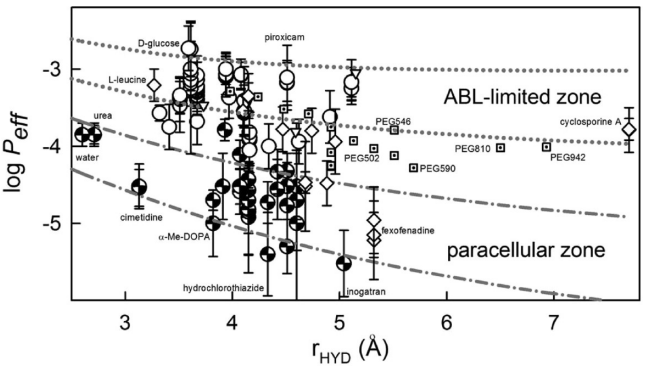

Figure 6. The plot of log P_{eff} as a function of the size of molecules. The compounds analyzed to be predominantly paracellular are indicated with checkered symbols. The molecules which were analyzed to be predominantly ABL-limited are indicated by circle symbols. The transcellular class of compounds is distributed in the central section of the plot, largely between the dot and dot−dash curves, and are indicated by diamond symbols. The outliers are indicated with squares (PEGs) and triangles (quercetin-3.4′-diglucoside, L-DOPA, cephalexin).

The GOF of 1.3 suggests that the biophysical model matches the precision of the of the human P_{eff} data very well, and further improvement in the model would be of dubious gain, given that the human jejunal P_{eff} data have relatively high interindividual variability.[3] Table 4 lists the observed and calculated P_{eff} values. Figure 5 shows the corresponding plot of observed vs calculated log P_{eff}. The zero-weighted PEG P_{eff} data (unfilled symbols, Figure 5) showed consistently high positive residuals, 0.6 −1.3 log units.

Refined Effective Surface Area Expansion Factor. On the basis of the drug subset P_{eff} data refinement, the best-fit surface area expansion factor, k_{VF}, is 33.5 ± 9.8. This compares favorably with the estimate from the classical histological studies, where the value is about 30.[34,55−57] In contrast to the insights gained from anaesthetized rodent studies,[35] it appears that in *unanaesthetized* human subjects, possibly the full mucosal surface area of the jejunum is available for absorption, without apparent bias according to the lipophilicity of the drug. This is really a surprising and unexpected outcome of our study.

Transport Analysis for Drugs in the Human Jejunum. Figure 6 shows a plot of log P_{eff} of the 119 compounds as a function of the size of molecules. The compounds analyzed to be predominantly paracellular are indicated with checkered symbols. These are generally the low permeability compounds. They are grouped in the "paracellular zone," bounded by the dot−dash curves. The molecules which were analyzed to be predominantly ABL-limited are indicated by circle symbols. Most of these are near the top of the plot and are roughly bounded by the dot curves of the "ABL-limited zone." The transcellular class of compounds is distributed in the central section of the plot, largely between the dot and dot−dash curves, and are indicated by diamond symbols. The outliers are indicated with squares (PEGs) and triangles (quercetin-3.4′-diglucoside, L-DOPA, cephalexin).

In Figure 7, the 53 compounds are grouped into the three classes (ABL-limited transcellular, transcellular, and paracellular), each molecule represented by a pie chart showing the relative contributions from the three mechanisms. The numerical quantities within each chart refer to the average P_{eff} values (10^{-4} cm s^{-1}) and the human absolute bioavailability percentage.

Paracellular Route. Nearly half of the molecules whose human permeability has been reported appear to permeate predominantly via the paracellular route in the jejunum (Figure 7). This appears not to have been anticipated in the original P_{eff} studies, where only urea and creatinine are commonly designated paracellular, subject to solvent drag.[1−3,61] Our novel approach appears to have revealed new insights concerning the apportionment of some of the mechanisms of transport. Because of the low porosity of the cellular barrier, the compounds in the paracellular set are naturally low permeable, and their absolute oral absorption is not expected to be high. Of the 25 compounds in this class, 13 are uncharged molecules and 5 are cations. It is noteworthy that PEG942 has no likely option but to penetrate by the paracellular route, even though its molecular weight is nearly 1000 Da. Inspection of the molecules in this set indicates that the paracellular route is clearly available to molecules whose MW exceeds 300 Da. But the permeability coefficients of these molecules are near the bottom of the P_{eff} scale and are associated predominantly with hydrophilic or large molecules. The apparent presence of the "secondary" junction pores ($\varepsilon/\delta_2 = 0.027$ cm^{-1}) does afford an "escape" route out of the intestine, albeit a small one, for very large molecules by these size-unrestricted holes in the intestinal wall. After all, their P_{eff} values were measured as nonzero. Interestingly, enaliprilat, terbutaline, and atenolol, designated as paracellular here, are not subject to solvent-drag effects and had been classified as transcellular.[3] As evidence of the transcellular mechanism, it was pointed out by Lennernäs[3] that atenolol can be a competitor to P-glycoprotein substrates, a process believed to require the permeation across the mucosal membrane because the active site in the membrane is on the inner leaflet side. Similarly, terbutaline is thought to be transcellular because it is metabolized in the gut wall and thus must first pass across the mucosal membrane.[1−3] These observations are not inconsistent with our findings, where there is a transcellular contribution for atenolol and terbutaline (cf. Figure 7), albeit not a large one.

The transport process is complex and can simultaneously accommodate more than one mechanism for most molecules but in differing relative amounts, as indicated in Figure 7. The above atenolol and terbutaline transcellular processes could be sensitive to pH effects, increasingly favored at pH above 6.5, given the pK_a values of the compounds. Because

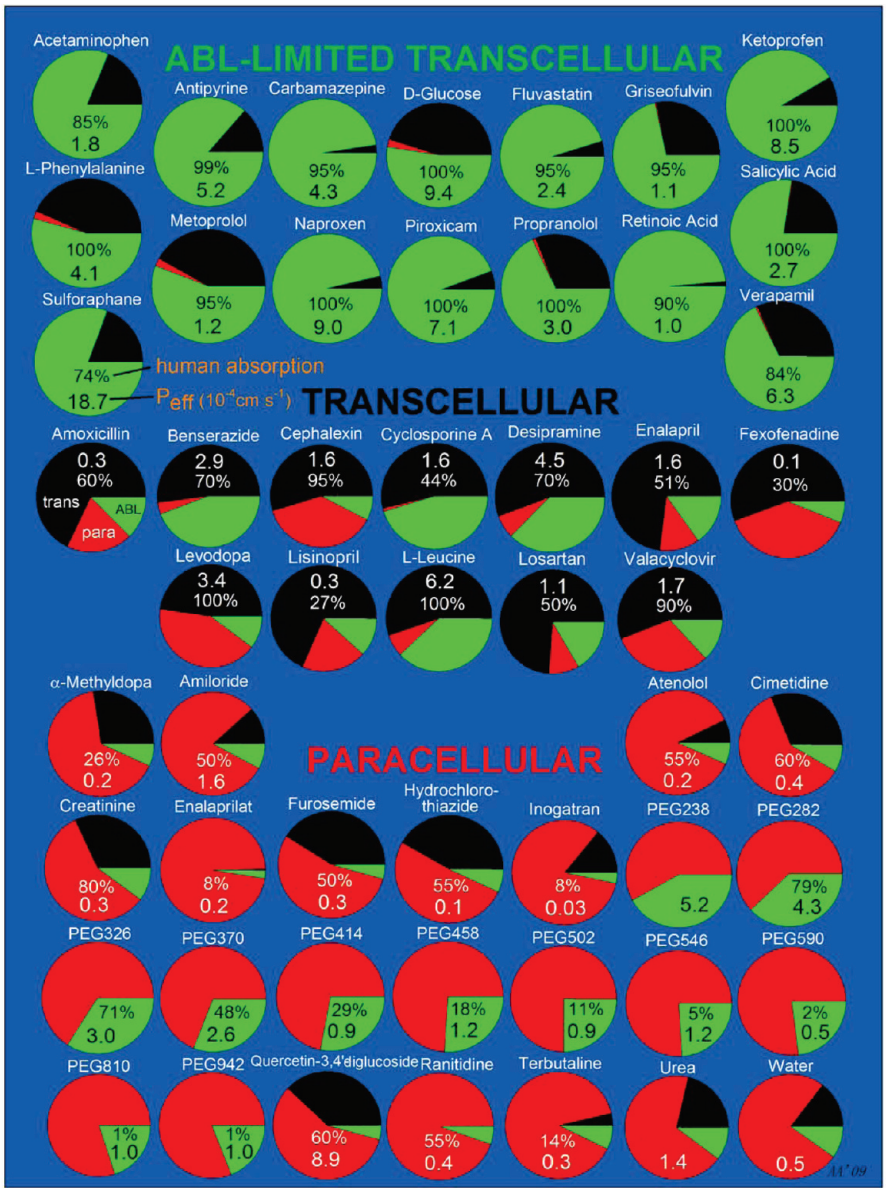

Figure 7. The 53 compounds grouped into the three classes: ABL-limited transcellular, transcellular, and paracellular. Each molecule is represented by a pie chart showing the relative contributions from the three classes (amoxicillin has legend). The numerical quantities within each chart refer to the average P_{eff} values (10^{-4} cm s^{-1}) and the human absolute bioavailability percentage.

some symport carriers are in part driven by pH gradients, there may be various murky issues concerning pH effects in the P_{eff} data that may play a role in some of the carrier-mediated or low permeable ionizable drugs. It is noteworthy that the pH in the crypts can be higher than that in the vicinity of the villus tips.[107] The model developed here could be easily modified to test the sensitivity of the tested compounds to local changes in pH, and this deserves further investigation.

The current opinion is that the paracellular diffusion is considered a minor intestinal transport route for drug molecules larger than MW 300 Da. Our study would recommend that the statement can be augmented to say that compounds *whose human absorption is* $>50\%$ are not likely to be transported by the paracellular route unless the MW $<$ 300 Da (cf. Table 1 and Figure 7; molecule **3** in Figure 9).[105]

ABL-Limited Transcellular Route. A little less than a third of the compounds in the P_{eff} set are ABL-limited in the effective permeability, according to calculations here. This high fraction was not anticipated. The current opinion is that the thickness of the jejunal ABL is 40−150 μm, smaller than previously assumed at 700−1000 μm.[3] However, at least some of the supportive evidence is based on "smooth tube" calculation of P_{eff}, where indeed the "effective" thickness calculates to be a small number.[52] In the current study, the best-fit physical thickness of the ABL based on the in situ perfusion data (Table 3) is estimated to be 4675 ± 1812 μm. This value may not be so inappropriate, given the dimensions of the *distended* segment of the jejunum during the experimental measurements (Figure 1), and it compares favorably to the 2800 μm ABL thickness predicted by the Johnson−Amidon[60] smooth-tube hydrodynamic model. Fasted-state in vivo conditions have a flattened intestinal tube, and the ABL thickness may indeed be in line with the older model with h_{ABL} 700−1000 μm. This would be consistent with the expected thickness of the mucus layer (Figure 1). Of the 16 compounds predicted to be in the ABL-limited class (Figure 7), six are uncharged molecules and six are anions. Most of the compounds are near the top of the P_{eff} scale, as expected.

The Caco-2 permeability-pH profile for retinoic acid (Figure 4) reveals a surprising effect of putative micelles migrating slowly through the stagnant water layers (as indicated by the unexpectedly low P_{ABL}), whereas in the membrane phase, the permeability of retinoic acid is very high (high values of P_c). For low soluble molecules (which have a tendency to form aggregates), such distensions of transport speed may be more common than suspected.[109] Permeability measurements as a function of pH[54,64,66−68,72,74−76,83,91,96,109] are useful in recognizing such anomalies and even in some cases recognizing the presence of carrier-mediated transport from the patterns of pH dependence.[54] However, the micelle effect may be an artifact in how both the in vitro and in vivo assays are performed, namely in simple buffer solutions. In the presence of components of biorelevant media (e.g., bile salts, lecithin), aggregates that form in simple buffer solutions can break down to monomeric species, presumably then associated with the lipid components of the biorelevant media.[109]

Transcellular Route. The prevailing thought in the current literature suggests that most of the compounds in the human measurements cross the intestinal barrier by the transcellular route. The present study supports this view. However, our results suggest a complicated picture. Of the compounds evaluated, 53% predominantly cross the mucosal membrane by either the ABL-limited transcellular or by the direct transcellular route. Of these, about half fall into the latter (unhindered) category. Being below the ABL and above the paracellular limits, these compounds would naturally possess "medium" permeability. Of the 12 compounds predicted to be in the normal transcellular class, surprisingly, half are zwitterions. The preponderance of zwitterions in this class suggests that some may be carrier-mediated in their mode of transport because zwitterions usually have low oral absorption (< 50%), as suggested by a recent study.[105] But whether this happens in vivo has not been openly published.

Polyethylene Glycol Permeability is in a Class by Itself. Although PEGs can be used as valuable markers for monitoring pathological states leading to breaches in the intestinal barrier (e.g., Crohn's disease), in the present study, it is evident that the permeability characteristics of PEGs cannot be described with the same parameters as those associated with drug-like molecules of comparable molecular weights (cf., Table 3). Their transport mechanism appears to be in a class by itself.

Polyethylene glycols are hydrophilic molecules, with log P_{OCT} ranging from −2.0 for PEG194 to −4.3 for PEG942 (Table 5).[36] Because such compounds are expected to permeate cell monolayers by the paracellular mechanism, the estimate of their transcellular permeability, P_c[6.5], is challenging to determine from in vitro P_{app} measurements. Artursson et al.[61] characterized the Caco-2 permeation of the monodisperse series, PEG194−502, and compared the results to the corresponding human intestinal permeability values based on the data of Chadwick et al.[4] (recalculated[61] from disappearance rates). PEGs are small flexible oligomers, facilely changing between ordered helical and random coil conformations,[99] possibly exhibiting Browning motion distinctly different from that of drug-like molecules. Cross-sectional diameter or radius of gyration may be better hydrodynamic models of size[61,106] than the radii predicted from the Stokes−Einstein equation. According to Ruddy and Hadzija,[100] the measured hydrodynamic radii of PEGs can be approximated from molecular weight, according to

$$r_{HYD}^{PEG}(\text{Å}) = 0.29\text{MW}^{+0.454} \quad (9)$$

Table 5. Properties of Polyethylene Glycols [a]

compd	log P_{OCT}	log P_c	r_{HYD}^{PEG} (Å)	r_S (Å) [b]	D_{aq} (10^{-6} cm^2 s^{-1})
PEG194	*−1.98*	−7.64	3.34		10.5
PEG238	−2.21	−7.76	3.48	4.51	9.9
PEG282	*−2.54*	−7.94	3.76	4.87	8.9
PEG326	*−2.76*	−8.06	4.01	5.15	8.2
PEG370	−3.08	−8.23	4.25	5.47	7.7
PEG414	*−3.12*	−8.25	4.47	5.78	7.2
PEG458	*−3.27*	−8.34	4.69	6.03	6.8
PEG502	−3.40	−8.41	4.88	6.27	6.5
PEG546	*−3.53*	−8.50	5.07	6.55	6.2
PEG590	*−3.65*	−8.56	5.25	6.77	6.0
PEG810	*−4.13*	−8.83	6.07	7.89	5.1
PEG942	*−4.28*	−8.95	6.50		4.8

[a] log P_{OCT} are the octanol−water partition coefficients taken from the literature[36] or interpolated (italic). The Caco-2 log P_c are based on analysis of Caco-2 data (eq 7, with k_{VF} = 1), using the relationship log P_c = −6.57 + 0.54 log P_{OCT}, with coefficients determined elsewhere.[58] Equation 9 was used to calculate the hydrodynamic radii of PEGs, r_{HYD}^{PEG}. The aqueous diffusivity coefficients, D_{aq}, were calculated using eq 2 with "effective" MW defined such that eq 5 produces r_{HYD}^{PEG} values corresponding to those of eq 9. [b] Effusion theory-based analysis.[106]

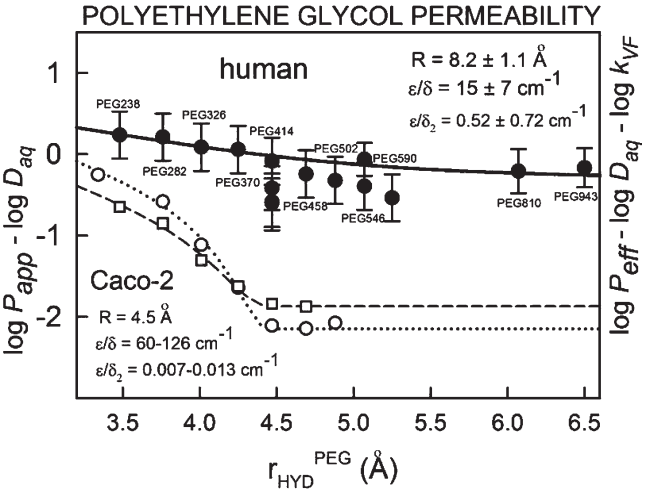

Figure 8. For the series of PEGs studied, the plot of log(P_{eff} k_{VF}^{-1} D_{aq}^{-1}) for human jejunal data (k_{VF} = 33.5) and log(P_{app} D_{aq}^{-1}) for Caco-2 data vs r_{HYD}^{PEG}. The unfilled circles[61] and squares[102] refer to Caco-2 P_{app} data. The solid symbols correspond to human P_{eff} data.

Equation 9 calculates radii that are about 0.5 Å smaller than those calculated from the Sutherland−Stokes−Einstein expression, eq 5 (cf. Tables 1 and 5).

Pramauro and Pelezetti[101] noted that rod-like molecules have an enhanced tendency to permeate through water-filled cylindrical channels, compared to smaller ellipsoidal or spherical molecules, due to hydrodynamic fluid-shear alignment expected in such rod-in-cylinder diffusion processes. Both Artursson et al.[61] and Watson et al.[102] observed that the apparent permeability of PEGs was substantially higher than that of drug-like molecules of comparable molecular weight. The latter investigators attributed this to their smaller hydrodynamic radii (e.g., for comparable molecular weights, mannitol has r = 4.1 Å, whereas PEG194 has r = 3.3 Å). It was proposed that a small population of size-unrestricted pores may exist within the junctions (perhaps in the triangular gaps[103] of three-cell junction regions, Figure 1 inset), coexisting with a large population of size-restricted

pores (e.g., in regular adjoining-cell junctions). This bimodal diffusion model is consistent with the interpretation of log P_{app} vs r_{HYD} plots for PEGs.[61,102,103] The possibility of dual pore size distribution in intestinal junctions has been considered by a number of investigators.[40,45,102−104,106]

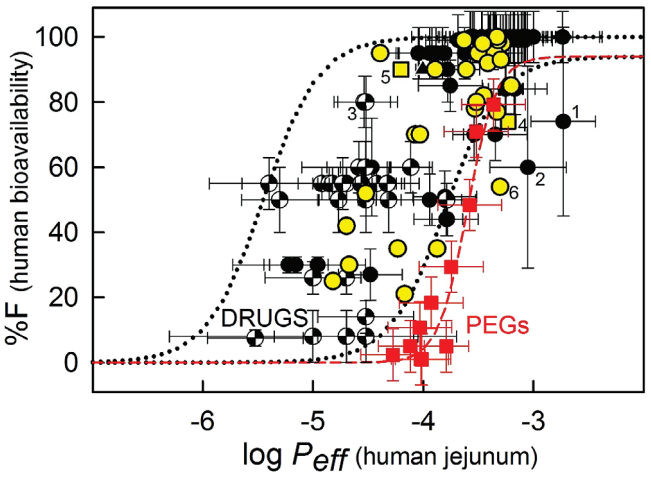

Figure 9. Plot of the absolute human bioavailability vs log P_{eff}. The measured drug P_{eff} values are represented by solid circles, checkered circles (paracellular set), triangle (retinoic acid); the measured PEGs are represented by red squares. The yellow circles and squares represent P_{eff} of "test" compounds calculated from the refined parameters in Table 3. The indexes: 1 = sulforaphane, 2 = quercetin-3,4′-diglucoside, 3 = creatinine, 4 = sulforaphane based on Caco-2 prediction, 5 = retinoic acid based on Caco-2 prediction, 6 = diclofenac. The curves are indicated by $\%F = A/[1 + \exp(-(\log P_{eff} - B)/C]$; left dotted curve: $A = 100$, $B = -5.45$, $C = 0.25$; right dotted curve: $A = 94$, $B = -3.8$, $C = 0.25$; dashed curve: $A = 94$, $B = -3.6$, $C = 0.13$.

In our earlier interlaboratory PEG Caco-2 data analysis,[58] we found that PEGs were substantially more permeable than drug-like molecules of the same size. The PEG human data here were reanalyzed separately (15 P_{eff} values), leading to refined parameters (cf. Table 3) which were significantly different from those describing the drug molecules subset (99 P_{eff} values). For example, the PEG-human parameters indicated a small junction pore radius (8.2 Å) compared to the value refined in the drug subset (11.2 Å). Apparently, a much higher density of junction pores (both size-restricted, ε/δ, and size-independent, ε/δ_2) are accessible by the PEGs than that available to drug molecules (Table 3).

For a series of PEGs, Figure 8 shows the plot of $\log(P_{eff}\, k_{VF}^{-1}\, D_{aq}^{-1})$ for human jejunal data and $\log(P_{app}\, D_{aq}^{-1})$ for Caco-2 data vs r_{HYD}^{PEG} (eq 9). For the PEG-Caco-2 profile, $k_{VF} = 1$. For the PEG-human profile, the k_{VF} factor was taken as 33.5 (Table 3). The unfilled circle and square symbols refer to Caco-2 P_{app} data from Artrusson et al.[61] and Watson et al.,[102] respectively. The solid symbols correspond to human P_{eff} data.[4,17,18,23,29,61] Table 5 lists the Caco-2 transcellular permeability, log $P_c^{6.5}$, determined as a linear function of log P_{OCT}[58] in the analysis of Caco-2 data using eq 7 (with $k_{VF} = 1$).

As is evident in Figure 8, the permeability of the human jejunum to PEGs is much higher than that of the Caco-2 model, particularly for the high-MW oligomers, even when normalized for the surface area expansion. Table 3 summarizes the refined transport parameters for the PEG series. The capacity of the size-independent pores, ε/δ_2, for the human jejunum is about 40−74 times higher than that of the Caco-2 monolayer (cf. Figure 7).

Table 6. Absolute Bioavailability, Predicted P_{eff}, and Cell Permeation Properties of the Test Molecules

compd	%*F*	%*F* refs	predicted log P_{eff}	predominant charge	log $P_c^{6.5}$ Caco-2/MDCK	Caco-2/MDCK refs
acyclovir	21	105	−4.17	0	−5.87	65, 66, 71, 77, 94
caffeine	98	112	−3.28	0	−4.09	68, 69
cetirizine	90	105	−3.89	±	−5.32	81
chloramphenicol	82	112	−3.45	0	−4.47	65
chlorpheniramine	35	112	−3.87	+	−5.35	81
ciprofloxacin	70	105	−4.07	±,+	−5.62	114
dexamethasone	78	112	−3.53	0	−4.65	62, 99
diazepam	95	112	−3.35	0	−4.15	69
diclofenac	54	112	−3.30	−	−3.67	68
digoxin	70	112	−4.03	0	−5.45	65, 69
etoposide	52	112	−4.52	0	−6.16	68, 84
famotidine	42	105	−4.70	+,0	−7.36	90
fluorescein	99	112	−3.63	−	−4.91	115
glipizide	95	112	−3.50	−	−4.50	68
ibuprofen	85	112	−3.21	−	−3.10	68
indomethacin	99	112	−3.32	−	−3.18	68
isoxicam	100	112	−3.33	−	−3.79	68
lincomycin	25	112	−4.82	+	−7.76	84
nadolol	30	112	−4.67	+	−7.60	66, 96
norfloxacin	35	105	−4.23	±,+	−5.87	114
ofloxacin	90	105	−3.61	±,+	−4.85	114
pantoprazole	77	113	−3.33	−	−3.12	65
propylthiouracil	85	112	−3.20	0	−3.66	62
quinine	80	112	−3.52	+	−4.66	65, 84
sotalol	95	112	−4.39	+	−6.26	62
sparfloxacin	92	105	−3.41	±,+	−4.23	114
trimethoprim	98	112	−3.46	+	−4.56	62, 66
warfarin	93	112	−3.30	−	−3.32	62, 69, 87
sulforaphane	74	30	−3.23	0	−3.85	this work
retinoic acid	90	3	−4.22	−	−4.27[a]	this work

[a] Assumed the transport across the stagnant water layer and the paracellular channels as micelles.

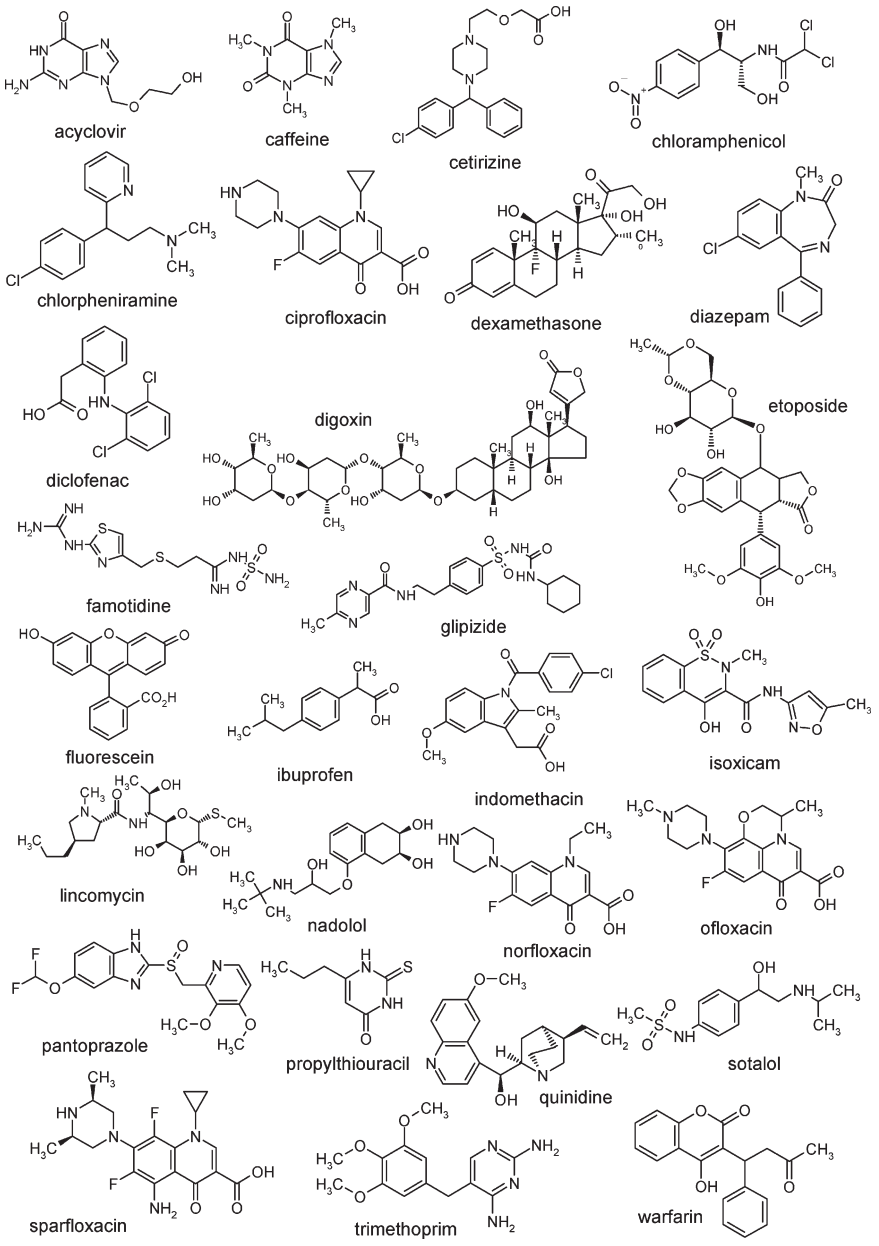

Figure 10. Stuctures of the 28 "test" drugs.

The PEG-indicated pores in the Caco-2 system, 4.5 Å, are smaller than those in the human jejunum, 8.2 Å. The PEG-indicated size-restricted "normal" junctions in the human jejunum have 4−8 times less capacity, ε/δ, than that of the Caco-2 model (cf. Figure 8). From the analysis of the Caco-2 PEG data, the paracellular route accounted for 90−98% of the total transport. In the case of PEG human data, the paracellular route accounted from about 58% (PEG194) to 81% (PEG942) of the total transport, with the aqueous boundary layer resistance accounting for the remaining contribution to transport.

The "Leakiness" of the Human Jejunum Compared to that of in Vitro Models. If the PEG series were used to characterize the paracellular property of membrane barriers, the human jejunum would be considered leakier than Caco-2 monolayers, especially for large PEGs (cf. Figure 8). However, the PEGs may not ideally represent the permeation properties of drug-like molecules, as is evident here and as was discussed elsewhere.[58,61,102,103] The interlaboratory study[58] of the leakiness and size-exclusion of Caco-2 and MDCK cell lines, based on 14 studies taken from eight laboratories, suggested a unified way (using "isoparacellular profiles") of comparing leakiness of drug-like molecules using mannitol as a reference compound. The drug subset human jejunal parameters (Table 3) predict mannitol to have a $P_{eff} = 0.38 \times 10^{-4}$ cm s^{-1}, or $P_{app} = 1.1 \times 10^{-6}$ cm s^{-1} (taking $k_{VF} = 1$ for Caco-2). This is about the middle of the leakiness scale.[58] Several groups have a similar reference value:[58] P_{app} 1.1×10^{-6} cm s^{-1} (MDCK-NCI: Garberg et al.[69]), P_{app} 1.7×10^{-6} cm s^{-1} (Caco-2: Adson et al.,[43] Knipp et al.[108]), P_{app} 1.8×10^{-6} cm s^{-1} (Caco-2: Garberg et al.,[69] Liang et al.[86]). The cell lines developed at the former Upjohn company[43,69] and the University of Kansas[108] appear to best match the paracellular characteristics of the human jejunum when the surface area expansion factor, k_{VF}, is taken into account. Thus, it appears that the human jejunum is *not* leakier than "typical" Caco-2/MDCK cell lines. This is indeed quite surprising.

Applications of the Biophysical Model. Figure 9 shows a plot of the human bioavailability (%F) against measured

human P_{eff} of the 41 drugs (black filled/checkered circles, triangle). The molecules indicated by checkered circles are those identified in Figure 7 as being predominantly paracellular. All the bioavailability values and the estimated errors were taken from various publications.[3,30,105,112−117] It can be seen that the $\%F$ and the P_{eff} data generally follow a sigmoid shape, which is consistent with the literature.[1−3] The spread of points between the two dotted curves is substantial and reflects the high interindividual variability in the measured P_{eff} values. Notwithstanding, still there are two outliers, namely sulforaphane (**1**) and quercetin-3,4′-diglucoside (**2**). The absolute bioavailability data of these two molecules in human are not available in open literature. The $\%F$ data quoted in Table 1 and Figure 9 were estimates from the perfusion experiments.[30] However, the absorption of quercetin-3,4′-diglucoside is also complicated by the fact that the molecule may be metabolized by lactase phlorizin hydrolyase before it is transported through intestinal epithelial layer.[30] It is plausible that the hydrolyzed product, quercetin, is the predominant permeant across the epithelial layer, which may further complicate the in vivo absorption. (Quercetin is expected to be more permeable than its diglucoside derivative.) However, the possibility of an uptake transporter process cannot be dismissed; quercetin 4′-β-glucoside has been shown to be a substrate of the sodium-dependent glucose transporter, SGLT1, in both Caco-2 cells and in SGLT1-transfected Chinese hamster ovary G6D3 cell line.[118] As for sulforaphane, it has been suggested that glutathione conjugation reaction could occur in the epithelial cell.[30] This may introduce increased uncertainties to the measured human P_{eff} data. It is interesting to note that the predicted human P_{eff} value based on our measured Caco-2 permeability (yellow square, **4**: Figure 9) fits better with the $\%F$ data than the measured human P_{eff} data (black circle, **1**: Figure 9). A similar observation is seen for another molecule, retinonic acid, where the measured human P_{eff} value is indicated by the yellow square, **5**, and black triangle to the right of it. This is in good agreement with the Caco-2 based P_{eff} prediction.

Next, attention is turned to the PEGs data, which are symbolized as red squares in Figure 9. As discussed above, the transport characteristics of PEGs appear to be different from other drug molecules of comparable size. Generally, the P_{eff} values of PEGs are higher, but their bioavailability values are lower than that of the drug molecules with similar size (especially for larger oligomers). The absolute bioavailability values of PEGs were taken from refs 17 and 110. It is noted that the bioavailability of PEGs is estimated by the urine excretion method. However, this may be underestimated to some extent, as the method ignored other routes of elimination.

To evaluate the P_{eff} prediction model developed in this study, a further set 28 drug molecules were selected, with structures shown in Figure 10. We have carefully selected these molecules, which have low to moderate in vivo clearance in human[111] (i.e., do not show significant metabolic liability) and with published Caco-2/MDCK permeability data. Table 6 shows the bioavailability, the predicted human P_{eff}, and the Caco-2 permeability of the 28 test molecules. In this set of molecules, 17% are ampholytes, 25% are bases, 29% are acids, and 29% are neutral. As shown in Figure 9, these molecules (in yellow circles) also exhibit a sigmoid relationship between the bioavailability and the predicted human P_{eff} values. The trend is similar to that of the 41 drug molecules (black solid/checkered circles, triangle) with measured human P_{eff} data. The largest outlier is diclofenac (**6**). The overall comparison may suggest that the predicted human P_{eff} values generated using our biophysical model are comparable to the measured human P_{eff} values, and can be used for ranking human bioavailability of drug molecules. We anticipate that the P_{eff} predictions from our biophysical model would be a reliable and yet inexpensive alternative to intestinal perfusion studies.

Conclusion

We have studied the human jejunal permeability data (119 P_{eff} values, 53 compounds) taken mainly from the publications of Lennernäs and Amidon groups. The data have been analyzed by a weighted nonlinear regression based on a biophysical model, which takes into consideration the permeabilities across the aqueous boundary layer, the villus-fold surface area expansion factor, paracellular, and transcellular permeabilities. It has been shown that the transcellular permeability used in our biophysical model could be taken from in vitro cell-based permeability data, such as Caco-2/MDCK cell lines, pooled from various publications. The surface area expansion has been shown to be in the region of 30, which is good agreement with the expected increase in the mucosal surface in the human jejunum (from a smooth surface) based on anatomical evidence. Except for a few molecules where the permeation processes are complicated by metabolic issues, the predictions by our biophysical model agree with the available human jejunal permeability data within experimental uncertainty.

This investigation showed that the unstirred water layer thickness in the in situ perfusion experiments is much greater than had been commonly thought, the mucosal surface area in humans is apparently fully accessible to drug absorption, in contrast to anesthetized rodent studies, and the relative "leakiness" of the human jejunum is not so different from that observed in a number of Caco-2 studies, when the surface area expansion factor is taken into account.

Our analysis on the P_{eff} data of PEGs, where the transport mechanism is predominately paracellular, suggests that the permeability characteristics are somewhat different from drug-like molecules of similar size, and two types of junction pores, namely size/charge-restricted, and size independent, are accessible by the PEGs. The performance of our biophysical model has been evaluated using a test set of drug molecules with published Caco-2/MDCK permeability data. The predicted P_{eff} values of this test set show a sigmoid correlation with the human absolute bioavailability, and the agreement is similar to the drug molecules in the Lennernäs−Amidon set where measured P_{eff} data are available. We have demonstrated that the human P_{eff} values can be predicted with confidence by the biophysical model developed in this study using measured Caco-2/MDCK permeability as input parameter. It is envisaged that this could be a reliable and yet inexpensive alternative to human perfusion studies.

Experimental Section

Chemicals Used. Hanks' balanced salts solution (HBSS) were purchased from Invitrogen (Carlsbad, CA). Sulforaphane (purity ≥90% by HPLC) and 13-cis-retinoic acid (isotretinoin; purity ≥98% by HPLC) were purchased from Sigma-Aldrich (St. Louis, MO) and were used without further purification. DMSO spectrophotometric grade was obtained from VWR

(used to make stock solutions of sulforaphane and retinoic acid).

Cell Culture Method. Caco-2 cells (passage no. 19) were purchased from the American Type Culture Collection (Manassas, VA). Stocks of Caco-2 cells were maintained in Dulbecco's Modified Eagle Medium (DMEM; cat. no. 10-010-CV, Mediatech, Manassas, VA) plus 10% certified fetal bovine serum (Gibco, cat. no. 16000, lot 378738; Grand Island, NY), 0.1 mM nonessential amino acids, 2 mM L-glutamine, and 100 IU mL^{-1} penicillin and 100 μg mL^{-1} streptomycin (Mediatech, cat. no. 30-002-CI). Cells were propagated in 75 cm^2 T-flasks (Cell Treat) at 37 °C in an incubator with 5% CO_2. Monolayers were subcultured when they reached about 60−80% confluence. Feeding medium was changed every two to three days.

The cells were seeded at a density of 66000 cells cm^{-2} onto microporous polycarbonate membranes (0.4 μm pores, 0.135 porosity) in 24-well HTS Transwell plates (Costar no. 3396, Corning, NY). The culture medium was changed 48 h after seeding to remove cell debris and dead cells; afterward, the medium was changed every other day for 3 weeks.

Monolayer Integrity. TEER measurements were taken in the feeding solution before (489 ± 41 Ω cm^2) and after permeability assays (349 ± 83 Ω-cm^2). All wells were considered acceptable. Atenolol at pH 5.5 was used as indicator of the paracellular junction leakiness. On prior occasions, the acceptable performance of the present batch of cells was further verified using propranolol (aqueous boundary layer marker), metoprolol, and indomethacin (cell permeability markers).

Transport Media. Gradient pH conditions were used for retinoic acid; the donor wells contained pH 6.0, 6.5, 7.0, 7.4, or 8.0 buffers, while all the receiver wells contained a pH 7.4 buffer. For the nonionizable sulforaphane, donor and receiver solutions consisted of a pH 7.4 buffer. The permeability media buffers made either from Hanks' balanced salts solution (HBSS), containing Ca^{2+}, Mg^{2+}, and 5.56 mM glucose, modified by adding 25 mM HEPES (adjusted to pH 7.0, 7.4, or 8.0 by adding standardized NaOH or HCl) or by adding 10 mM MES (adjusted to pH 6.0 or 6.5 by adding standardized NaOH or HCl). After 30 min preincubation with sample-free buffer, solutions were removed from the inserts (top compartments) and replaced with the samples solutions at corresponding pH values. Solutions in the bottom compartments were not replaced after preincubation.

The test compounds (from 10 mM DMSO stock solutions) were prepared in a particular buffer to a final concentration of 50 μM each for sulforaphane and retinoic acid. Sulforaphane did not precipitate at that concentration. However, retinoic acid showed partial precipitation, particularly pronounced at pH 6.0, but its solutions were filtered before being placed into the donor compartments. An 800 μL aliquot of blank buffer was applied to the bottom (receiver) wells, and 150 μL of the test compounds were dosed on the apical side and incubated at 37 °C (5% CO_2, 90% relative humidity, orbital shaker speed at 384 rpm, rev min^{-1}). After 60 min, all samples were transferred from the inserts and the wells into 96-well plastic UV plates (Greiner) for UV analysis.

Sample Analysis. Both the donor and acceptor solutions were assayed for the amount of material present, using the PAMPA Evolution instrument (*p*ION), by comparison with the UV spectrum (250−500 nm) obtained from pure reference standards. The strengths of the UV signal were acceptable, and there was no need to do further LC/MS analysis. Mass balance, as described below, was used to determine the amount of material recovered in the donor and receiver solutions at the end of the assay.[97]

Apparent Permeability Calculation. The traditional formula used to define P_{app} generally assumes a sink condition (i.e., no back flux) and that cell retention of the permeant is zero (i.e., 100% mass balance). Since many of today's medicinal chemistry programs produce poorly soluble drug candidates, the simple formula can be inaccurate. To remedy some of this, the generalized gradient pH apparent permeability coefficient, P_{app}, can be calculated as[97]

$$P_{app} = -\frac{2.303 V_D}{A \cdot t} \cdot \left(\frac{1}{1+r_a}\right) \cdot \log_{10}\left[1 - \left(\frac{1+r_a^{-1}}{1-R_{cell}}\right) \cdot \left(\frac{C_R(t)}{C_D(t=0)}\right)\right] \quad (10)$$

where V_D = donor well volume (0.15 cm^3), V_R = receiver well volume (0.80 cm^3), A = filter surface area (0.33 cm^2), t = incubation time (3600 s), and C_R and C_D (mol cm^{-3}) are the receiver and donor well concentrations of the permeant as a function of time, respectively; the sink asymmetric ratio (due to gradient pH) is defined as[97]

$$r_a = \frac{V_D}{V_R} \cdot \left(\frac{P_{app}^{R \to D}}{P_{app}^{D \to R}}\right) \quad (11)$$

and the equilibrium cell retention factor, R_{cell}, refers to the *mole* amount of the permeant "lost" from the aqueous phase as a fraction of the total mole amount.[97] If the "lipid" cell volume, V_{mem}, were known, then R_{cell} could be converted to the buffer-monolayer partition coefficient, PC, as

$$PC = \left(\frac{R_{cell}}{1-R_{cell}}\right) \cdot \left(\frac{V_D + V_R}{V_{mem}}\right) \quad (12)$$

The detail steps in solving eq 10 have been described elsewhere.[97] The PAMPA Evolution software (*p*ION INC) was used to perform the calculations.

Acknowledgment. All of the Caco-2 measurements reported here were performed by the *p*ION Biopharma Services group, with the skilled efforts of Oksana Tsinman (*p*ION INC) and Dr. Raphael Nir (SBH Sciences) greatly appreciated. Helpful discussions with Drs. Hans Lennernäs (Uppsala University, Sweden), Jennifer B. Dressman (Goethe University, Germany), Kiyohiko Sugano (Pfizer, UK), and Sibylle Neuhoff (Simcyp, UK) are gratefully acknowledged.

References

(1) Lennernäs, H. Animal data: the contributions of the Ussing chamber and perfusion systems to predicting human oral drug delivery in vivo. *Adv. Drug Delivery Rev.* **2007**, *59*, 1103–1120.
(2) Lennernäs, H. Modeling gastrointestinal drug absorption requires more in vivo biopharmaceutical data: experience from in vivo dissolution and permeability studies in humans. *Curr. Drug Metab.* **2007**, *8*, 645–657.
(3) Lennernäs, H. Intestinal permeability and its relevance for absorption and elimination. *Xenobiotica* **2007**, *37*, 1015–1051.
(4) Chadwick, V. S.; Phillips, S. F.; Hofmann, A. F. Measurements of intestinal permeability using low molecular weight polyethylene glycols (PEG 400). II. Application to normal and abnormal permeability states in man and animals. *Gastroenterology* **1977**, *73*, 247–251.
(5) Vidon, S.; Evard, D.; Godbillo, J.; Rongier, M.; Duval, M.; Schoeller, J. P.; Bernier, J. J.; Hirtz, J. Investigation of drug absorption from the gastrointestinal tract of man. II. Metoprolol in the jejunum and ileum. *Br. J. Clin. Pharmacol.* **1985**, *19*, 107S–112S.
(6) Sutcliffe, F. A.; Riley, S. A.; Kaser-Liard, B.; Trunberg, L. A.; Rowland, M. Absorption of drugs from human jejunum and ileum. *Br. J. Clin. Pharmacol.* **1988**, *26*, 206P–207P.
(7) Lennernäs, H.; Ahrenstedt, O.; Hallgren, R.; Knutson, L.; Ryde, M.; Paalzow, L. K. Regional jejunal perfusion, a new in vivo approach to study oral drug absorption in man. *Pharm. Res.* **1992**, *9*, 1243–1451.
(8) Lennernäs, H.; Nilsson, D.; Aquilonius, S. M.; Ahrenstedt, O.; Knutson, L.; Paalzow, L. K. The effect of L-leucine on the absorption of levodopa, studied by regional jejunal perfusion in man. *Br. J. Clin. Pharmacol.* **1993**, *35*, 243–250.

(9) Gramatté, T.; el Desoky, E.; Klotz, U. Site dependent small intestinal absorption of ranitidine. *Eur. J. Clin. Pharmacol.* **1994**, *46*, 253–259.
(10) Gramatté, T.; Richter, K. Paracetamol absorption from different sites in the human small intestine. *Br. J. Clin. Pharmacol.* **1994**, *37*, 608–611.
(11) Gramatté, T. Griseofulvin absorption from different sites in the human small intestine. *Biopharmacol. Drug Disp.* **1994**, *15*, 747–759.
(12) Lennernäs, H.; Ahrenstedt, O.; Ungell, A.-L. Intestinal drug absorption during induced net water absorption in man; a mechanistic study using antipyrine, atenolol, and enalaprilat. *Br. J. Clin. Pharmacol.* **1994**, *37*, 589–596.
(13) Fagerholm, U.; Borgstrom, L.; Ahrenstedt, O.; Lennernäs, H. The lack of effect on induced net fluid absorption on the in vivo permeability of terbutaline in the human jejunum. *J. Drug Targeting* **1995**, *3*, 191–200.
(14) Lennernäs, H.; Knutson, L.; Knutson, T.; Lesko, L.; Salmonson, T.; Amidon, G. L. Human effective permeability data for furosemide, hydrochlorothiazide, ketoprofen and naproxen to be used in the proposed biopharmaceutical classification for IR-products. *Pharm. Res.* **1995**, *12*, 396.
(15) Lindahl, A.; Sandstrom, R.; Ungell, A.-L.; Abrahamsson, B.; Knutson, T. W.; Knutson, L.; Lennernäs, H. Jejunal permeability and hepatic extraction of fluvastatin in humans. *Clin. Pharmacol. Ther.* **1996**, *60*, 493–503.
(16) Lennernäs, H.; Nylander, S.; Ungell, A.-L. Jejunal permeability: a comparison between the Ussing chamber technique and the single-pass perfusion in humans. *Pharm. Res.* **1997**, *14*, 667–671.
(17) Söderholm, J. D.; Olaison, G.; Kald, A.; Tagesson, C; Sjodahl, R. Absorption profiles for polyethylene glycols after regional perfusion and oral load in healthy humans. *Dig. Dis. Sci.* **1997**, *42*, 853–857.
(18) Takamatsu, N.; Welage, L. S.; Idkaidek, N. M.; Liu, D.-Y.; Lee, P. I.-D.; Hayashi, Y.; Rhie, J. K.; Lennernäs, H.; Barnett, J.; Shah, V. P.; Lesko, L.; Amidon, G. L. Human intestinal permeability of piroxicam, propranolol, phenylalanine, and PEG400 determined by jejunal perfusion. *Pharm. Res.* **1997**, *14*, 1127–1132.
(19) Lennernäs, H. Human intestinal permeability. *J. Pharmacol. Sci.* **1998**, *87*, 403–410.
(20) Winiwarter, S.; Bonham, N. M.; Ax, F.; Hallberg, A.; Lennernäs, H.; Karlen, A. Correlation of human jejunal permeability (in vivo) of drugs with experimentally and theoretically derived parameters. A multivariate data analysis approach. *J. Med. Chem.* **1998**, *41*, 4939–4949.
(21) Fagerholm, U.; Nilsson, D.; Knutson, L.; Lennernäs, H. Jejunal permeability in umans in vivo and rats in situ: investigation of molecular size selectivity and solvent drag. *Acta Physiol. Scand.* **1999**, *165*, 315–324.
(22) Sandström, R.; Knutson, T. W.; Knutson, L.; Jansson, B.; Lennernäs, H. The effect of ketoconazole on the jejunal permeability and CYP3A metabolism of (R/s)-verapamil in humans. *Br. J. Clin. Pharmacol.* **1999**, *48*, 180–189.
(23) Takamatsu, N.; Kim, O.-N.; Welage, L. S.; Idkaidek, N. M.; Hayashi, Y.; Barnett, J.; Yamamoto, R.; Lipka, E.; Lennernäs, H.; Hussain, A.; Lesko, L.; Amidon, G. L. Human jejunal permeability of two polar drugs: cimetidine and ranitidine. *Pharm. Res.* **2001**, *18*, 742–744.
(24) Lennernäs, H.; Knutson, L.; Knutson, T.; Hussain, A.; Lesko, L.; Salmonson, T.; Amidon, G. L. The effect of amiloride on the in vivo effective permeability of amoxicillin in human jejunum: experience from a regional perfusion technique. *Eur. J. Pharm. Sci.* **2002**, *15*, 271–277.
(25) Sun, D.; Lennernäs, H.; Welage, L. S.; Barnett, J. L.; Landowski, C. P.; Foster, D.; Fleisher, D.; Lee, K. D.; Amidon, G. L. Comparison of human duodenum and Caco-2 gene expression profiles for 12000 gene sequence tags and correlation with permeability of 26 drugs. *Pharm. Res.* **2002**, *19*, 1400–1416.
(26) Tannergren, C.; Knutson, T.; Knutson, L.; Lennernäs, H. The effect of ketoconazole on the in vivo intestinal permeability of fexofenadine using a regional perfusion technique. *Br. J. Clin. Pharmacol.* **2003**, *55*, 182–190.
(27) Winiwarter, S.; Ax, F.; Lennernäs, H.; Hallberg, A.; Pettersson, C.; Karlen, A. Hydrogen bonding descriptors in the prediction of human in vivo intestinal permeability. *J. Mol. Graphics Modell.* **2003**, *21*, 273–287.
(28) Tannergren, C.; Petri, N.; Knutson, L.; Hedeland, M.; Bondesson, U.; Lennernäs, H. Multiple transport mechanisms involved in the intestinal absorption and first-pass extraction of fexofenadine. *Clin. Pharmacol. Ther.* **2003**, *74*, 423–436.
(29) Chiu, Y.-Y.; Higaki, K.; Neudeck, B. L.; Barnett, J. L.; Welage, L. S.; Amidon, G. L. Human jejunal permeability of cyclosporin A: influence of surfactants on P-glycoprotein efflux in Caco-2 cells. *Pharm. Res.* **2003**, *20*, 749–756.
(30) Petri, N.; Tannergren, C.; Holst, B.; Mellon, F. A.; Bao, Y.; Plumb, G. W.; Bacon, J.; O'Leary, K. A.; Kroon, P. A.; Knutson, L.; Forsell, P.; Eriksson, T.; Lennernäs, H.; Williamson, G. Absorption/metabolism of sulforaphane and quercetin, and regulation of phase II enzymes, in human jejunaum in vivo. *Drug Metab. Dispos.* **2003**, *31*, 805–813.
(31) Knutson, T.; Fridblom, P.; Ahlstroem, H.; Magnusson, A.; Tannergren, C.; Lennernäs, H. Increased understaniding of intestinal drug permeability determinined by the LOC-I-GUT approach using multislice computed tomography. *Mol. Pharm.* **2009**, *6*, 2–10.
(32) Wilson, J. P. Surface area of the small intestine in man. *Gut* **1967**, *8*, 618–621.
(33) Moog, F. The lining of the small intestine. *Sci. Am.* **1981**, *245* (11), 154–176.
(34) Madara, J. L. Functional morphology of epithelium of the small intestine. In *Handbook of Physiology, Section 6: The Gastrointestinal System*; Schultz, S. G., Ed.; American Physiological Society: Bethesda, 1991; pp 83−119.
(35) Yamashita, S.; Tanaka, Y.; Endoh, Y.; Taki, Y.; Sakane, T.; Nadai, T.; Sezaki, H. Analysis of drug permeation across Caco-2 monolayer: implications for predicting in vivo drug absorption. *Pharm. Res.* **1997**, *14*, 486–491.
(36) Collett, A.; Walker, D.; Sims, E.; He, Y.-L.; Speers, P.; Ayrton, J.; Rowland, M.; Warhurst, G. Influence of morphmetric factors on quantitation of paracellular permeability of intestinal epithelia in vitro. *Pharm. Res.* **1997**, *14*, 767–773.
(37) Oliver, R. E.; Jones, A. F.; Rowland, M. What surface of the intestinal epithelium is effectively available to permeating drugs? *J. Pharm. Sci.* **1998**, *87*, 634–639.
(38) Ungell, A.-L.; Nylander, S.; Bergstrand, S.; Sjöberg, Å.; Lennernäs, H. Membrane transport of drugs in different regions of the intestinal tract of the rat. *J. Pharm. Sci.* **1998**, *87*, 360–366.
(39) Fleisher, D. Biological transport phenomena in the gastrointestinal tract: cellular mechanisms. In *Transport Processes in Pharmaceutical Systems*; Amidon, G. L., Lee, P. I., Topp, E. M., Eds.; Marcel Dekker, Inc., New York, 2000; pp 147−184.
(40) Marcial, M. A.; Carlson, S. L.; Madara, J. L. Partitioning of paracellular conductance along the ileal and crypt-villus axis: a hypothesis based on structural analysis with detailed consideration of tight junction structure−function relationships. *J. Membr. Biol.* **1984**, *80*, 59–70.
(41) Madara, J. L.; Pappenheimer, J. R. Structural basis for physiological regulation of paracellular pathways in intestinal epithelia. *J. Membr. Biol.* **1987**, *100*, 149–164.
(42) Hollander, D. The intestinal permeability barrier. A hypothesis as to its regulation and involvement in Crohn's disease. *Scand. J. Gastroenterol.* **1992**, *27*, 721–726.
(43) Adson, A.; Raub, T. J.; Burton, P. S.; Barsuhn, C. L.; Hilgers, A. R.; Audus, K. L.; Ho, N. F. H. Quantitative approaches to delineate paracellular diffusion in cultured epithelial cell monolayers. *J. Pharm. Sci.* **1994**, *83*, 1529–1536.
(44) Tanaka, Y.; Yaki, Y.; Sakane, T.; Nadai, T.; Sezaki, H.; Yamashita, S. Characterization of drug transport through tight junctional pathway in Caco-2 monolayer: comparison with isolated rat jejunum and colon. *Pharm. Res.* **1995**, *12*, 523–527.
(45) Fine, K. D.; Santa Ana, C. A.; Porter, J. L.; Fordtran, J. S. Effect of changing intestinal flow rate on a measurement of intestinal permeability. *Gastroenterology* **1995**, *108*, 983–989.
(46) Thomson, A. B. R.; Dietschy, J. M. Derivation of the equations that describe the effects of unstirred water layers on the kinetic parameters of active transport processes in the intestine. *J. Theor. Biol.* **1977**, *64*, 277–294.
(47) Komiya, I.; Park, J. Y.; Kamani, A.; Ho, N. F. H.; Higuchi, W. I. Quantitative mechanistic studies in simultaneous fluid flow and intestinal absorption using steroids as model solutes. *Int. J. Pharm.* **1980**, *4*, 249–262.
(48) Högerle, M. L.; Winne, D. Drug absorption by the rat jejunum perfused in situ. Dissociation from the pH partition theory and the role of microclimate pH and unstirred layer. *Naunyn-Schmiedeberg's Arch. Pharmacol.* **1983**, *322*, 249–255.
(49) Shimada, T. Factors affecting the microclimate pH in rat jejunum. *J. Physiol.* (*London*) **1987**, *392*, 113–127.
(50) Levitt, M. D.; Furne, J. K.; Stocchi, A; Anderson, B. W.; Levitt, D. G. Physiological measurements of luminal stirring in the dog and human small bowl. *J. Clin. Invest.* **1990**, *86*, 1540–1547.
(51) Chiou, W. L. Effect of 'unstirred' water layer in the intestine on the rate and extent of absorption after oral administration. *Biopharm. Drug Disp.* **1994**, *15*, 709–717.

(52) Fagerholm, U.; Lennernäs, H. Experimental estimation of the effective unstirred water layer thickness in the human jejunum, and its importance in oral drug absorption. *Eur. J. Pharm. Sci.* **1995**, *3*, 247–253.
(53) Ho, N. F. H.; Raub, T. J.; Burton, P. S.; Barsuhn, C. L.; Adson, A.; Audus, K. L.; Borchardt, R. Quantitative approaches to delineate passive transport mechanisms in cell culture monolayers. In *Transport Processes in Pharmaceutical Systems*; Amidon, G. L., Lee, P. I., Topp, E. M., Eds.; Marcel Dekker: New York, NY, 2000; pp 219−316.
(54) Avdeef, A.; Artursson, P.; Neuhoff, S.; Lazarova, L.; Grasjö, J.; Tavelin, S. Caco-2 permeability of weakly basic drugs predicted with the Double-Sink PAMPA pK_a^{flux} method. *Eur. J. Pharm. Sci.* **2005**, *24*, 333–349.
(55) Desesso, J. M.; Jacobson, C. F. Anatomical and physiological parameters affecting gastrointestinal absorption in humans and rats. *Food Chem. Toxicol.* **2001**, *39*, 209–228.
(56) Pappenheimer, J. R.; Michel, C. C. Role of microcirculation in intestinal absorption of glucose: coupling of epithelial with endothelial transport. *J. Physiol.* **2003**, *553*, 561–574.
(57) Desesso, J. M.; Williams, A. L. Contrasting the gastrointestinal tracts of mammals: factors that influence absorption. *Annu. Rep. Med. Chem.* **2008**, *43*, 353–371.
(58) Avdeef, A. Leakiness and size exclusion of paracellular channels in cultured epithelial cell monolayers—interlaboratory comparison. *Pharm. Res.* **2010**, *27*, 480–489.
(59) Sugano, K. Introduction to computational oral absorption simulation. *Expert Opin. Drug Metab. Toxicol.* **2009**, *5*, 259–293.
(60) Johnson, D. A.; Amidon, G. L. Determination of intrinsic membrane transport parameters from perfused intestine experiments: a boundary layer approach to estimating the aqueous and unbiased membrane permeabilities. *J. Theor. Biol.* **1988**, *131*, 93–106.
(61) Artursson, P.; Ungell, A.-L.; Löfroth, J.-E. Selective paracellular permeability in two models of intestinal absorption: cultured monolayers of human intestinal epithelial cells and rat intestinal segments. *Pharm. Res.* **1993**, *10*, 1123–1129.
(62) Irvine, J. D.; Takahashi, L.; Lockhart, K.; Cheong, J.; Tolan, J. W.; Selick, H. E.; Grove, J. R. MDCK (Madin−Darby canine kidney) cells: a tool for membrane permeability screening. *J. Pharm. Sci.* **1999**, *88*, 28–33.
(63) Walter, E.; Janich, S.; Roessler, B. J.; Hilfinger, J. M.; Amidon, G. L. HT29-MTX/Caco-2 cocultures as an in vitro model for the intestinal epithelium: in vitro−in vivo correlation with permeability data from rats and humans. *J. Pharm. Sci.* **1996**, *85*, 1070–1076.
(64) Alsenz, J.; Haenel, E. Development of a 7-day, 96-well Caco-2 permeability assay with high throughput direct UV compound analysis. *Pharm. Res.* **2003**, *20*, 1961–1969.
(65) von Richter, O.; Glavinas, H.; Krajcsi, P.; Liehner, S.; Siewert, B.; Zech, K. A novel screening strategy to identify ABCB1 substrates and inhibitors. *Naunyn-Schmiedeberg's Arch. Pharmacol.* **2009**, *379*, 11–26.
(66) Thiel-Demby, V. E.; Humphreys, J. E.; St. John Williams, L. A.; Ellens, H. M.; Shah, N; Ayrton, A. D.; Polli, J. W. Biopharmaceutics Classification System: validation and learnings of an in vitro permeability assay. *Mol. Pharmaceutics* **2009**, *6*, 11–18.
(67) Laitinen, L.; Kangas, H.; Kaukonen, A. M.; Hakala, K.; Kotiaho, T.; Kostianen, R.; Hirvonen, J. N-in-One permeability studies of heterogeneous sets of compounds across Caco-2 cell monolayers. *Pharm. Res.* **2003**, *20*, 187–197.
(68) Lee, K.-J.; Johnson, N.; Castelo, J.; Sinko, P. J.; Grass, G.; Holme, K.; Lee, Y.-H. Effect of experimental pH on the in vitro permeability in intact rabbit intestines and Caco-2 monolayer. *Eur. J. Pharm. Sci.* **2005**, *25*, 193–200.
(69) Garberg, P.; Ball, M.; Borg, N.; Cecchelli, R.; Fenart, L.; Hurst, R. D.; Lindmark, T.; Mabondzo, A.; Nilsson, J. E.; Raub, T. J.; Stanimirovic, D.; Terasaki, T.; Oberg, J.-O.; Osterberb, T. In vitro models for the blood−brain barrier. *Toxicol. In Vitro* **2009**, *19*, 299–334.
(70) Wang, Q.; Strab, R.; Kardos, P.; Ferguson, C.; Li, J.; Owen, A.; Hidalgo, I. J. Application and limitation of inhibitors in drug−transporter interaction studies. *Int. J. Pharm.* **2008**, *356*, 12–18.
(71) Rege, B. D.; Yu, L. X.; Hussain, A. S.; Polli, J. E. Effect of common excipients on Caco-2 transport of low-permeability drugs. *J. Pharm. Sci.* **2001**, *90*, 1776–1786.
(72) Adson, A.; Burton, P. S.; Raub, T. J.; Barsuhn, C. L.; Audus, K. L.; Ho, N. F. H. Passive diffusion of weak organic electrolytes across Caco-2 cell monolayers: uncoupling the contributions of hydrodynamic, transcellular, and paracellular barriers. *J. Pharm. Sci.* **1995**, *84*, 1197–1204.
(73) Neuhoff, S.; Ungell, A.-L.; Zamora, I.; Artursson, P. pH-dependent bidirectional transport of weakly basic drugs across Caco-2 monolayers: implications for drug−drug interactions. *Pharm. Res.* **2003**, *20*, 1141–1148.
(74) Raeissi, S. D.; Li, J.; Hidalgo, I. J. The role of an α-amino group on H^+-dependent transepithelial transport of cephalosporins in Caco-2 cells. *J. Pharm. Pharmacol.* **1999**, *51*, 35–40.
(75) Pade, V.; Stavchansky, S. Estimation of the relative contributions of the transcellular and paracellular pathway to the transport of passively absorbed drugs in the Caco-2 cell culture model. *Pharm. Res.* **1997**, *14*, 1210–1215.
(76) Palm, K.; Luthman, K.; Ros, J.; Grasjö, J.; Artursson, P. Effect of molecular charge on intestinal epithelial drug transport: pH-dependent transport of cationic drugs. *J. Phamacol. Exp. Ther.* **1999**, *291*, 435–443.
(77) Yee, S. In vitro permeability across Caco-2 cells (colonic) can predict in vivo (small intestine) absorption in man—fact or myth? *Pharm. Res.* **1997**, *14*, 763–766.
(78) Zhao, R.; Raub, T. J.; Sawada, G. A.; Kasper, S. C.; Bacon, J. A.; Bridges, A. S.; Pollack, G. M. Breast cancer resistance protein interacts with various compounds in vitro, but plays a minor role in substate efflux at the blood−brain barrier. *Drug Metab. Dispos.* **2009**, *37*, 1251–1258.
(79) Karlsson, J.; Ungell, A.-L.; Grasjö, J.; Artursson, P. Paracellular drug transport across intestinal epithelia: influence of charge and induced water flux. *Eur. J. Pharm. Sci.* **1999**, *9*, 47–56.
(80) Hilgendorf, C.; Spahn-Langguth, H.; Regardh, C. G.; Lipka, E.; Amidon, G. L.; Langguth, P. Caco-2 vs Caco-2/HT29-MTX co-cultured cell lines: permeabilities via diffusion, inside- and outside-directed carrier-mediated transport. *J. Pharm. Sci.* **2000**, *89*, 63–75.
(81) Obradovic, T.; Dobson, G. G.; Shingaki, T.; Kungu, T.; Hidalgo, I. J. Assessment of the first and second generation antihistamine brain penetration and role of P-glycoprotein. *Pharm. Res.* **2007**, *24*, 318–327.
(82) Petri, N.; Tannergren, C.; Rungstad, D.; Lennernas, H. Transport characteristics of fexofenadine in the Caco-2 cell model. *Pharm. Res.* **2004**, *21*, 1398–1404.
(83) Phillips J. E.; Ruell J. Unpublished data, Apr **2003**.
(84) Wang, Q.; Rager, J. D.; Weinstein, K.; Kardos, P. S.; Dobson, G. L.; Li, J.; Hidalgo, I. J. Evaluation of the MDR-MDCK cell line as a permeability screen for the blood−brain barrier. *Int. J. Pharm.* **2005**, *288*, 349–359.
(85) Yazdanian, M.; Glynn, S. L.; Wright, J. L.; Hawi, A. Correlating partitioning and Caco-2 cell permeability of structurally diverse small molecular weight compounds. *Pharm. Res.* **1998**, *15*, 1490–1494.
(86) Liang, E.; Chessic, K.; Yazdanian, M. Evaluation of an accelerated Caco-2 cell permeability model. *J. Pharm. Sci.* **2000**, *89*, 336–345.
(87) Aungst, B. J.; Nguyen, N. H.; Bulgarelli, J. P.; Oates-Lenz, K. The influence of donor and reservoir additives on Caco-2 permeability and secretory transport of HIV protease inhibitors and other lipophilic compounds. *Pharm. Res.* **2000**, *17*, 1175–1180.
(88) Korjamo, T.; Heikkinen, A. T.; Waltari, P.; Mönkkönen, J. The asymmetry of the unstirred water layer in permeability experiments. *Pharm. Res.* **2008**, *25*, 1714–1722.
(89) Karlsson, J.; Artursson, P. A method for the determination of cellular permeability coefficients and aqueous boundary layer thickness in monolayers of intestinal epithelial (Caco-2) cells grown in permeable filter chambers. *Int. J. Pharm.* **1991**, *71*, 55–64.
(90) Gan, L.-S. L.; Yanni, S.; Thakker, D. R. Modulation of the tight junctions of the Caco-2 cell monolayers by H2-antagonists. *Pharm. Res.* **1998**, *15*, 53–57.
(91) Neuhoff, S.; Ungell, A.-L.; Zamora, I.; Artursson, P. pH-dependent passive and active transport of acidic drugs across Caco-2 cell monolayers. *Eur. J. Pharm. Sci.* **2005**, *25*, 211–220.
(92) Hilgers, A. R.; Conradi, R. A.; Burton, P. S. Caco-2 cell monolayers as a model for drug transport across the intestinal mucosa. *Pharm. Res.* **1990**, *7*, 902–910.
(93) Levin, V. A. Relationship of octanol/water partition coefficient and molecular weight to rat brain capillary permeability. *J. Med. Chem.* **1980**, *23*, 682–684.
(94) Katragadda, S.; Jain, R.; Kwatra, D.; Hariharan, S.; Mitra, A. K. Pharmacokinetics of amino acid ester prodrugs of acyclovir after oral administration: interaction with the transporters on Caco-2 cells. *Int. J. Pharm.* **2008**, *362*, 93–101.
(95) Abbott, N. J. Prediction of blood−brain barrier permeation in drug discovery from in vivo, in vitro and in silico models. *Drug Discovery Today: Technol.* **2004**, *1*, 407–416.
(96) Yamashita, S.; Furubayashi, T.; Kataoka, M.; Sakane, T.; Sezaki, H.; Tokuda, H. Optimized conditions for prediction of intestinal drug permeability using Caco-2 cells. *Eur. J. Pharm. Sci.* **2000**, *10*, 195–204.

(97) Avdeef, A. *Absorption and Drug Development*; Wiley-Interscience: New York, 2003; pp 22−66.
(98) *ACD/Labs log P Prediction Program* (*v3.0*); Advanced Chemistry Development: Toronto, Canada.
(99) Huen, G.; Breitkreutz, J. Structures and molecular attributes of polyethylene glycols. *Pharmazie* **1994**, *49*, 562–566.
(100) Ruddy, S. B.; Hadzija, B. W. Iontophoretic permeability of polyethylene glycols through hairless rat skin: application of hydrodynamic theory for hindered transport through liquid-filled pores. *Drug Des. Discovery* **1992**, *8*, 207–224.
(101) Pramauro, E.; Pelzetti, E. *Surfactants in Analytical Chemistry*; Elsevier: Amsterdam, 1996; p 423.
(102) Watson, C. J.; Rowland, M.; Warhurst, G. Functional modeling of tight junctions in intestinal cell monolayers using polyethylene glycol oligomers. *Am. J. Cell Physiol.* **2001**, *281*, C388–C397.
(103) Van Itallie, C. M.; Holmes, J.; Bridges, A.; Gookin, J. L.; Coccaro, M. R.; Proctor, W.; Colegio, O. R.; Anderson, J. M. The density of small tight junction pores varies among cell types and is increased by expression of claudin-2. *J. Cell Sci.* **2008**, *121*, 298–305.
(104) Goswami, T.; Jasti, B. R.; Li, X. Estimation of the theoretical pore sizes of the porcine oral mucosa for permeation of hydrophilic permeants. *Arch. Oral Biol.* **2009**, *54*, 577–582.
(105) Tam, K. Y.; Avdeef, A.; Tsinman, O.; Sun, N. The permeation of amphoteric drugs through artificial membranes—an in combo absorption model based on paracellular and transmembrane permeability. *J. Med. Chem.* **2010**, *53*, 392–401.
(106) Linnankoski, J.; Mäkelä, J.; Palmgren, J.; Mauriala, T.; Vedin, C.; Ungell, A.-L.; Lazorova, L.; Artursson, P.; Urtti, A.; Yliperttula, M. Paracellular porosity and pore size of the human intestinal epithelium in tissue and cell culture models. *J. Pharm. Sci.* **2009**, *99*, 2166–2175.
(107) Daniel, H.; Neugerbauer, B.; Kratz, A.; Rehner, G. Localization of acid microclimate along intestinal villi of rat jejunum. *Am. J. Physiol.* **1985**, *248*, G293–G298.
(108) Knipp, G. T.; Ho, N. F. H.; Barsuhn, C. L.; Borchardt, R. T. Paracellular diffusion in Caco-2 cell monolayers: effect of perturbation on the transport of hydrophilic compounds that vary in charge and size. *J. Pharm. Sci.* **1997**, *86*, 1105–1110.
(109) Avdeef, A.; Kansy, M.; Bendels, S.; Tsinman, K. Absorption-excipient-pH classification gradient maps: sparingly-soluble drugs and the pH partition hypothesis. *Eur. J. Pharm. Sci.* **2008**, *33*, 29–41.
(110) He, Y. L.; Murby, S.; Warhurst, G. L.; Walker, D.; Ayrton, J.; Eastmond, R.; Rowland, M. Species differences in size discrimination in the paracellular pathway reflected by oral bioavailability of poly(ethylene glycol) and D-peptides. *J. Pharm. Sci.* **1998**, *87*, 626–633.
(111) Obach, R. S.; Lombardo, F.; Waters, N. J. Trend analysis of a database of intravenous pharmacokinetic parameters in humans for 670 drug compounds. *Drug Metab. Dispos.* **2008**, *36*, 1385–1405.
(112) Hou, T.; Wang, J.; Zhang, W.; Xu, X. ADME evaluation in drug discovery. 6. Can oral bioavailability in humans be effectively predicted by simple molecular property-based rules? *J. Chem. Inf. Model.* **2007**, *47*, 460–463.
(113) Physician's Desk Reference, 63rd ed.; Thomson Reuters: Montvale, NJ, 2009.
(114) Bermejo, M.; Avdeef, A.; Ruiz, A.; Nalda, R.; Ruell, J. A.; Tsinman, O.; Gonzalez, I.; Fernandez, C.; Sanchez, G.; Garrigues, T. M.; Merino, V. PAMPA—a drug absorption in vitro model. 7. Comparing rat in situ, Caco-2, and PAMPA permeability of fluoroquinolones. *Eur. J. Pharm. Sci.* **2004**, *21*, 429–441.
(115) Berginc, K.; Zakelj, S.; Levstik, L.; Ursic, D.; Kristl, A. Fluorescein transport properties across artificial lipid membranes, Caco-2 cell monolayers and rat jejunum. *Eur. J. Pharm. Biopharm.* **2007**, *66*, 281–285.
(116) Sietsema, W. K. The Absolute Oral Bioavailability of Selected Drugs. *Int. J. Clin. Pharmacol. Ther. Toxicol.* **1989**, *27*, 179–211.
(117) Jones, R.; Connolly, P. C.; Klamt, A.; Diedenhofen, M. Use of surface charges from DFT calculations to predict intestinal absorption. *J. Chem. Inf. Model.* **2005**, *45*, 1337–1342.
(118) Walgren, R. A.; Lin, J.-T.; Kinne, R. K.-H.; Walle, T. Cellular uptake of dietary flavonoid quercetin 4′-β-glucoside by sodium-dependent glucose transporter SGLT1. *J. Pharmacol. Exp. Ther.* **2000**, *294*, 837–843.